Introduction: Basic Aspects of Fluorine in Chemistry and Biology

1

Unique Properties of Fluorine and Their Relevance to Medicinal Chemistry and Chemical Biology

Takashi Yamazaki, Takeo Taguchi, and Iwao Ojima

1.1 Fluorine-Substituent Effects on the Chemical, Physical and Pharmacological Properties of Biologically Active Compounds

The natural abundance of fluorine as fluorite, fluoroapatite, and cryolite is considered to be at the same level as that of nitrogen on the basis of the Clarke number of 0.03. However, only 12 organic compounds possessing this special atom have been found in nature to date (see Figure 1.1) [1]. Moreover, this number goes down to just five different types of compounds when taking into account that eight ω-fluorinated fatty acids are from the same plant [1]. [*Note:* Although it was claimed that naturally occurring fluoroacetone was trapped as its 2,4-dinitrohydrazone, it is very likely that this compound was fluoroacetaldehyde derived from fluoroacetic acid [1]. Thus, fluoroacetone is not included here.]

In spite of such scarcity, enormous numbers of synthetic fluorine-containing compounds have been widely used in a variety of fields because the incorporation of fluorine atom(s) or fluorinated group(s) often furnishes molecules with quite unique properties that cannot be attained using any other element. Two of the most notable examples in the field of medicinal chemistry are 9α-fluorohydrocortisone (an anti-inflammatory drug) [2] and 5-fluorouracil (an anticancer drug) [3], discovered and developed in 1950s, in which the introduction of just a single fluorine atom to the corresponding natural products brought about remarkable pharmacological properties. Since then, more than half a century has

Fluorine in Medicinal Chemistry and Chemical Biology Edited by Iwao Ojima

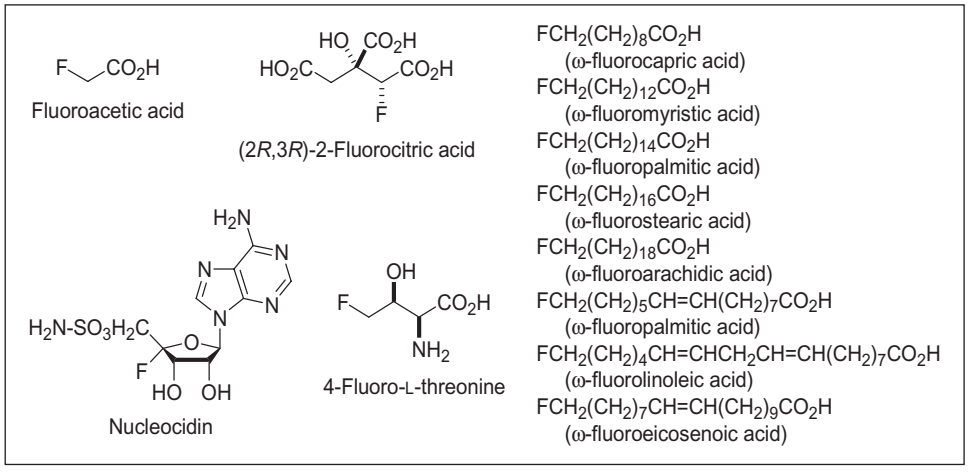

Figure 1.1 *Naturally occurring fluorine-containing compounds.*

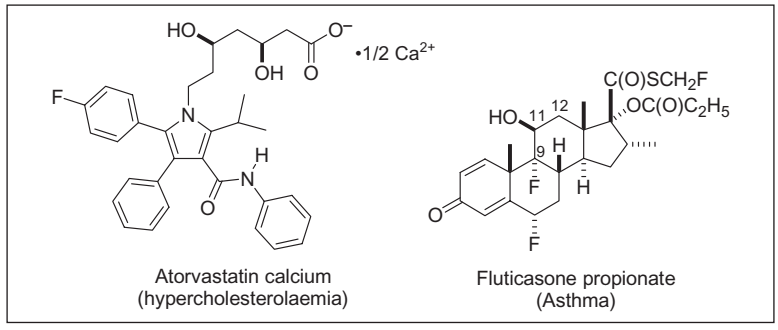

Figure 1.2 *Two fluorine-containing drugs.*

passed, and the incorporation of fluorine into pharmaceutical and veterinary drugs to enhance their pharmacological properties has become almost standard practice. In 2006, the best- and the second-best-selling drugs in the world were Lipitor® (atorvastatin calcium) by Pfizer/Astellas ($14.4 billion/year) and Advair®(U.S.A.)/Seretide®(E.U.) (a mixture of fluticasone propionate and salmeterol; only the former contains fluorine) by GlaxoSmithKline ($6.1 billion/year) which contain one and three fluorine atoms, respectively (see Figure 1.2) [4]. These fluorine-containing drugs are followed by risperidone (rank 10th, with one fluorine and $4.2 billion/year) for schizophrenia by Janssen, and lansoprazole (rank 17th, with a CF_3 moiety and $3.4 billion/year), a proton pump inhibitor, by Takeda/Abbott [4].

These huge successes of fluorine-containing drugs continue to stimulate research on fluorine in medicinal chemistry for drug discovery. It would not be an exaggeration to say

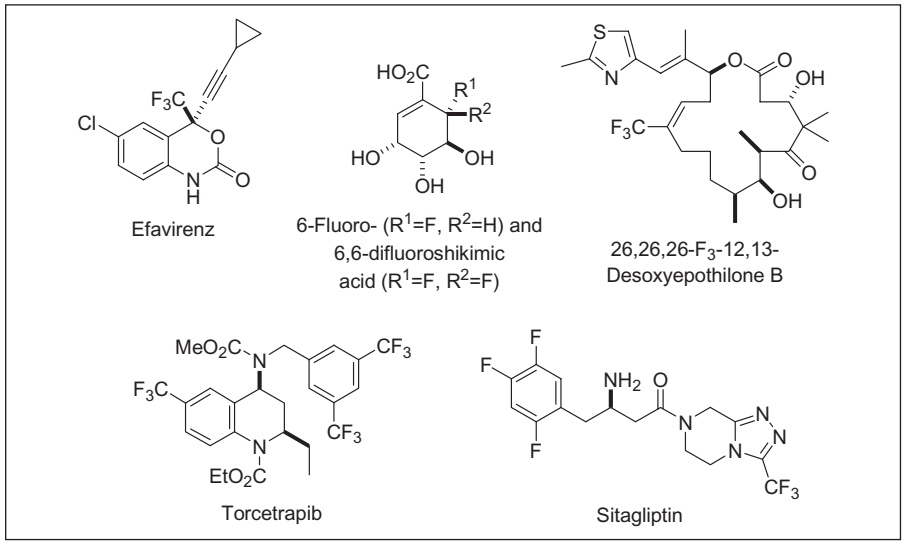

Figure 1.3 *Examples of fluorine-containing drugs and drug candidates.*

that currently every new drug discovery and development program without exception explores fluorine-containing drug candidates. Accordingly, a wide variety of fluorine-containing compounds based either on known natural products or on new skeletons have been synthesized and subjected to biological evaluation. In most cases, 1–3 fluorines are incorporated in place of hydroxyl groups or hydrogen atoms. Representative examples include efavirenz (CF_3) (HIV antiviral) [5], fluorinated shikimic acids (CHF or CF_2) (antibacterial) [6], and epothilone B analogue (CF_3) (anticancer) [7] (see Figure 1.3). In addition to these fluorine-containing drugs or drug candidates, a smaller number of fluorine-containing drugs include 6–9 fluorines in a molecule. For example, torcetrapib (a potent inhibitor of cholesterol ester transfer protein) possesses three CF_3 groups (Pfizer) [8], and sitagliptin (an antidiabetic for type 2 diabetes) has three fluorine atoms and one CF_3 group (Merck) [9] (see Figure 1.3).

In order to synthesize a variety of fluorine-containing biologically active compounds, development of efficient synthetic methods applicable to fluorine-containing organic compounds is necessary [10–19]. There is a strong demand for expansion of the availability of versatile fluorine-containing synthetic building blocks and intermediates to promote target-oriented synthesis as well as diversity-oriented synthesis. The limited availability of fluorochemicals for bioorganic and medicinal chemistry as well as pharmaceutical and agrochemical applications is mainly due to the exceptional properties and hazardous nature of fluorine and fluorochemical sources. Also, in many cases, synthetic methods developed for ordinary organic molecules do not work well for fluorochemicals because of their unique reactivity [10–19].

In this chapter, characteristic properties associated with the incorporation of fluorines or fluorine-containing groups to organic molecules are described in detail based on the most updated literature sources [20–32].

1.1.1 Mimic Effect and Block Effect

Table 1.1 summarizes representative physical properties of fluorine in comparison with other selected elements. As Table 1.1 clearly shows, the van der Waals (vdW) radius of fluorine is 1.47 Å [33] which is only 20% larger than that of hydrogen and much smaller than those of other halogens (Cl and Br are 46% and 54% larger than hydrogen, respectively). The C–F bond length in CH_3F is 1.382 Å, which is 0.295 Å longer than the methane's C–H bond, but 0.403 and 0.551 Å shorter than the C–Cl and C–Br bonds, respectively. Because of this similarity in size to hydrogen, it has been shown that microorganisms or enzymes often do not recognize the difference between a natural substrate and its analogue wherein a C–H bond of the substrate is replaced with a C–F bond. This observation is the basis of what is regarded as the "mimic effect" of fluorine for hydrogen.

One of the best-known examples is the behavior of fluoroacetic acid (CH_2FCO_2H) in the TCA (citrate acid or Krebs) cycle (see Scheme 1.1) [36]. As Scheme 1.1 illustrates, fluoroacetic acid is converted to fluoroacetyl-CoA (**1b**), following the same enzymatic transformation to the original substrate, acetic acid. Then, fluoroacetic acid is converted to (2*R*,3*R*)-fluorocitric acid (**2b**) by citrate synthase since this enzyme does not distinguish **1b** from acetyl-CoA (**1a**). In the next step, **2b** is dehydrated by aconitase to give (*R*)-fluoro-*cis*-aconitic acid (**3b**) in the same manner as that for the natural substrate **2a** to afford *cis*-aconitic acid (**3a**). In the normal TCA cycle, **3a** is hydroxylated to give isocitric acid (**4**), while **3b** undergoes hydroxylation-defluorination in an S_N2' manner to give (*R*)-hydroxy-*trans*-aconitic acid (**5**). It has been shown that the high affinity of **5b** for aconitase shuts down the TCA cycle, which makes **5b** as well as its precursors, fluoroacetic acid and **2b,** significantly toxic [36].

A number of protein structures determined by X-ray crystallography have been reported to date for the complexes of various enzymes with fluorine-containing substrate mimics or inhibitors bearing multiple fluorines. This strongly suggests that not only single fluorine displacement but also various fluorine-substitution patterns in substrate analogues

Table 1.1 *Representative physical data of selected elements [33–35]*

	Element (X)					
	H	C	O	**F**	Cl	Br
Electronegativity[a]	2.20	2.55	3.44	**3.98**	3.16	2.96
van der Waals radius[b] (Å)	1.20	1.70	1.52	**1.47**	1.75	1.85
H_3C–X bond length[a] (Å)	1.087	1.535[d]	1.425[e]	**1.382**	1.785	1.933
H_3C–X dissociation energy[c] (kcal/mol)	103.1	88.0[d]	90.2[e]	**108.1**	81.1	67.9
Ionization potential[a] (kcal/mol)	313.9	259.9	314.3	**402.2**	299.3	272.7
Electron affinity[a] (kcal/mol)	17.42	29.16	3.73	**78.52**	83.40	77.63

[a] Ref. [34].
[b] Ref. [33].
[c] Ref. [35].
[d] X = CH_3.
[e] X = OH.

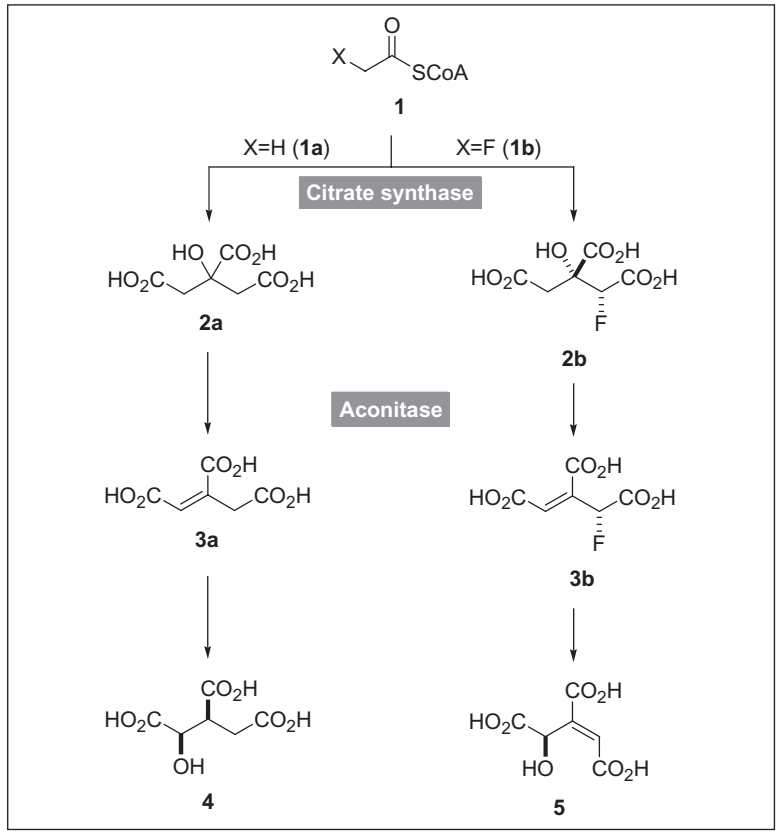

Scheme 1.1 *Conversion of acetyl-CoA and fluoroacetyl-CoA in the TCA cycle.*

or inhibitors could be adapted to biological systems in a molecular-recognition mode similar to that of the natural substrates [22, 37, 38].

Since the H_3C–*F* bond is stronger than that of H_3C–*H* by 5.0 kcal/mol (see Table 1.1), the replacement of a specific C–H bond with a C–F bond can effectively block metabolic processes via hydroxylation of C–H bonds, predominantly by the cytochrome P-450 family of enzymes. This function is referred to as the "block effect," and the strategic incorporation of fluorine(s) into metabolism site(s) has been widely used to prevent deactivation of biologically active substances *in vivo*. For example, it was found that the hydroxylation of the methylene moiety at the 24-position in the side-chain of vitamin D_3 (**6a**) was a critical deactivation step prior to excretion [39]. To block this undesirable metabolism, a strategic fluorine substitution was used; that is, a difluoromethylene group was introduced to the 24-position of **6b** [40], which indeed effectively blocked the hydroxylation at this site. The resultant **6c** was then hydroxylated enzymatically at the 1 position to give **7b**. 24,24-Difluoro-25-hydroxyvitamin D_3 (**6c**) was found to be slightly more potent than **6b**, and 24,24-difluoro-1,25-dihydroxyvitamin D_3 (**7b**) exhibited 5–10 times higher potency than **7a** [41] (see Scheme 1.2).

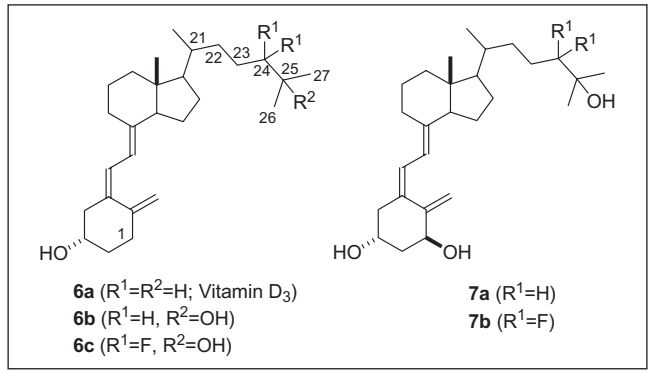

6a (R^1=R^2=H; Vitamin D_3)
6b (R^1=H, R^2=OH)
6c (R^1=F, R^2=OH)

7a (R^1=H)
7b (R^1=F)

Scheme 1.2 *24,24-Difluoro-25-OH-vitamin D_3 (**6c**) and 24,24-difluoro-1,25-dihydroxyvitamin D_3 (**7b**).*

In addition to the "mimic effect" and "block effect," introduction of just one fluorine substituent can induce electronic effects on its neighbors by affecting the electron density of functional groups such as hydroxyl and amino groups. This electronic effect decreases the pK_a value and Lewis basicity of these functional groups and retards their oxidation. For example, fluticasone propionate (see Figure 1.2) and related anti-inflammatory steroids contain fluorine at the 9α position. The role of the 9α-fluorine is to increase the acidity of the hydroxyl group at the 11 position, which promotes better binding to the enzyme active site and inhibits undesirable oxidation [42, 43].

1.1.2 Steric Effect of Fluorine and Fluorine-containing Groups

As Table 1.1 shows, fluorine is the second smallest element, with size approximately 20% larger than the smallest element, hydrogen. Table 1.2 summarizes four steric parameters for various elements and groups: (i) Taft steric parameters E_s [44], (ii) revised Taft steric parameters E_s' [45], (iii) Charton steric parameters υ [46], and (iv) *A* values [47]. The steric parameters, E_s, E_s', and υ are determined on the basis of relative acid-catalyzed esterification rates, while the *A* values are derived from the Gibbs free energy difference calculated from the ratios of axial and equatorial conformers of monosubstituted cyclohexanes by NMR.

As Table 1.2 shows, a stepwise substitution of a methyl group with fluorine gradually increases its bulkiness. For the bulkiness of CH_2F compared to CH_3, E_s, E_s', and υ values all show about 20% increase in size. For the bulkiness of CHF_2 and CF_3, however, the E_s values indicate 50% increase for CHF_2 and 90% increase for CF_3 in size as compared to CH_3, while the E_s' and υ values indicate only 30% and 70% increase in size, respectively.

In the case of *A* values, it is interesting to note that the first introduction of a fluorine atom into a methyl group leads to higher axial preference than that of a methyl group (i.e., CH_2F is regarded as smaller than CH_3), and the second fluorine substitution (i.e.,

Table 1.2 *Selected steric parameters of various elements and groups [44, 46–49]*

	$-E_s$[a]	$-E_s'$[a]	υ[b]	A[c] (kcal/mol)
H	0.00	0.00	0.00	0.00
F	0.46	0.55	0.27	0.15
CH_3	1.24	1.12	0.52	1.70
Cl	0.97	1.14	0.55	0.43
CH_3CH_2	1.31	1.20	0.56	1.75
CH_2F	1.48 (1.19)[d]	1.32 (1.18)[d]	0.62 (1.19)[d]	1.59[e] (0.94)[d]
Br	1.16	1.34	0.65	0.38
CHF_2	1.91 (1.54)[d]	1.47 (1.31)[d]	0.68 (1.31)[d]	1.85[e] (1.09)[d]
$(CH_3)_2CH$	1.71	1.60	0.76	2.15
CF_3	2.40 (1.94)[d]	1.90 (1.70)[d]	0.91 (1.75)[d]	2.37[f] (1.39)[d]
$(CH_3)_2CHCH_2$	2.17	2.05	0.98	–
$(CH_3)_3C$	2.78	2.55	1.24	4.89[e]

[a]Ref. [44].
[b]Ref. [46].
[c]Ref. [47].
[d]The ratio on the basis of the value of a CH_3 groups is shown in parentheses.
[e]Ref. [49].
[f]Ref. [48].

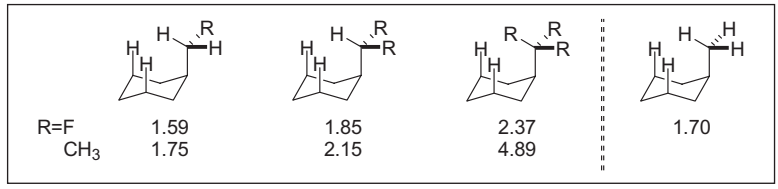

Figure 1.4 *Correlation of* A *values (kcal/mol) with 1,3-diaxial strains.*

CHF_2) causes a rather small increase in the *A* value. The *A* values of CH_2F and CHF_2 can be explained by taking into account a specific conformation of the axial conformers of monosubstituted cyclohexanes bearing these two substituents. As Figure 1.4 illustrates, the C–H of CH_2F and CHF_2 substituents occupies the *endo* position and bulkier fluorine(s) take(s) *exo* position(s) to minimize 1,3-diaxial strain. However, in the case of a spherical CF_3 substituent, a C–F inevitably takes the *endo* position, which increases the 1,3-diaxial strain. This would be the reason why the difference in *A* values between CF_3 and CHF_2 is considerably larger than that between CHF_2 and CH_2F. The same trend is observed for CH_3, CH_2CH_3, $CH(CH_3)_2$, and $C(CH_3)_3$ (see Figure 1.4) [50]. *A* values for other substituents have recently been reported: C_2F_5 (2.67), CF_3S (1.18), CF_3O (0.79), and CH_3O (0.49) [49].

The bulkiness of a CF_3 group has been estimated on the basis of comparison of rotational barriers along the biphenyl axis of 1,1′-disubstituted biphenyls **8a** to **8c** [51] as well as **9a** and **9b** [52]. These data clearly indicate that the bulkiness of a CF_3 group is similar to that of a $(CH_3)_2CH$ group (see Figure 1.5) [51–53].

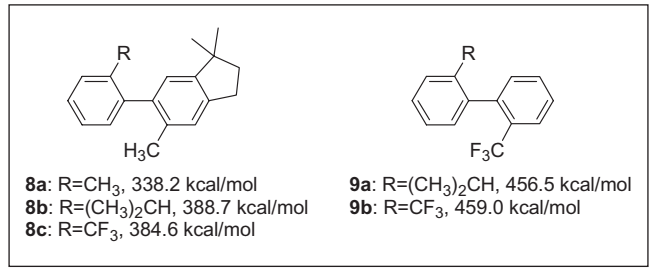

Figure 1.5 *Rotational barriers for **8** and **9**.*

Table 1.3 *Hansch hydrophobicity parameters for monosubstituted benzenes [54, 55]*

X in C_6H_5-X	π_X[a]	X in C_6H_5-X	π_X	X in C_6H_5-X	π_X
F	0.14	OCH_3	–0.02	$CH_3C(O)NH$-	–1.63
Cl	0.71	OCF_3	1.04	$CF_3C(O)NH$-	0.55
OH	–0.67	$CH_3C(O)$-	–1.27	CH_3SO_2-	–1.63
CH_3	0.56	$CF_3C(O)$-	0.08	CF_3SO_2-	0.55
CF_3	0.88				

[a] π_X: $\log P_X - \log P_H$ (octanol–water).

1.1.3 Lipophilicity of Fluorine and Fluorine-containing Groups

The absorption and distribution of a drug molecule *in vivo* are controlled by its balance of lipophilicity and hydrophilicity as well as ionization. Enhanced lipophilicity together with change in amine pK_a often leads to increase in blood–brain barrier (BBB) permeability or binding free energy through favorable partition between the polar aqueous solution and the less-polar binding site. It is generally conceived that incorporation of fluorine or fluorinated groups increases the lipophilicity of organic compounds, especially aromatic compounds. Table 1.3 shows selected Hansch π_X parameters [54, 55] for monosubstituted benzenes.

As Table 1.3 shows, fluorobenzene is slightly more lipophilic than benzene, but chlorobenzene is much more lipophilic. In a similar manner, CF_3-Ph is 57% more lipophilic than CH_3-Ph. The comparison of CF_3-Y-Ph and CH_3-Y-Ph (Y = O, CO, CONH, SO_2) reveals that CF_3-Y-Ph is substantially more lipophilic than CH_3-Y-Ph. In these CF_3-containing compounds, a strongly electron-withdrawing CF_3 group significantly lowers the electron density of the adjacent polar functional groups Y, which compromises the hydrogen-bonding capability of these functional groups with water molecules, and hence decreases hydrophilicity. Along the same lines, CF_3-benzenes with Lewis basic functionalities such as amine, alcohol, ether, carbonyl, and amide at the *ortho* or *para* position, decreases the hydrogen-bond accepting capability of these functionalities in an aqueous phase, which leads to increase in hydrophobicity and thus lipophilicity.

In contrast, the introduction of fluorine into aliphatic compounds results in decrease in lipophilicity. For example, pentane ($\log P = 3.11$) is more lipophilic than

Table 1.4 *log*P *values of straight-chain alkanols [57]*

Alcohols	X = H	X = F	$\Delta\log P_F - \log P_H$
	$\log P_H$	$\log P_F$	
CX_3CH_2OH	–0.32	0.36	0.68
$CX_3(CH_2)_2OH$	0.34	0.39	0.05
$CX_3(CH_2)_3OH$	0.88	0.90	0.02
$CX_3(CH_2)_4OH$	1.40	1.15	–0.25
$CX_3(CH_2)_5OH$	2.03	1.14	–0.89

1-fluoropentane ($\log P = 2.33$). Likewise, (3-fluoropropyl)benzene ($\Delta\log P = -0.7$) and (3,3,3-trifluoropropyl)benzene ($\Delta\log P = -0.4$) are considerably less lipophilic than propylbenzene [34]. In fact, the Hansch parameters π for CF_3 and CH_3 are 0.54 and 0.06, respectively, in aliphatic systems [56].

Table 1.4 shows selected $\log P$ values of straight-chain alkanols bearing a terminal CF_3 groups and comparisons with those of the corresponding nonfluorinated counterparts [57]. Trifluoroethanol is more lipophilic than ethanol ($\Delta\log P = -0.68$), which can be ascribed to the significant decrease in the basicity of the hydroxyl group by the strong electron-withdrawing effect of the CF_3 moiety. This strong through-bond σ-inductive effect of the CF_3 moiety extends up to three methylene inserts but diminishes beyond four. When the inductive effect of the CF_3 moiety does not affect the basicity of the hydroxyl group, reversal of relative lipophilicity is observed for 4-CF_3-butanol ($\Delta\log P = -0.25$) and 5-CF_3-pentanol ($\Delta\log P = -0.89$) as compared with butanol and pentanol, respectively. In the case of amines, a large enhancement of lipophilicity is observed, in general, when fluorine is introduced near to an amino group. This is attributed to the decrease in the amine basicity through the σ-inductive effect of fluorine, resulting in increase in the neutral amine component as opposed to the ammonium ion in equilibrium [58].

1.1.4 Inductive Effect of Fluorine and Fluorine-containing Groups

Since fluorine is the most electronegative element, it is natural that groups containing fluorine have unique inductive effects on the physicochemical properties of the molecules bearing them. For example, substantial changes in pK_a values of carboxylic acids, alcohols, or protonated amines are observed upon incorporation of fluorine into these molecules. Thus, when fluorine(s) and/or fluorine-containing group(s) are incorporated into bioactive compounds, these substituents will exert strong effects on the binding affinity for the receptors or target enzymes, biological activities, and pharmacokinetics.

Halogen substitution at the 2-position of acetic acid decreases the pK_a values in the order Br > Cl > F, which is qualitatively parallel to electronegativity (see Table 1.5). Thus, fluorine exerts the strongest effect ($\Delta pK_a = -2.17$ compared to 4.76 for acetic acid). Further substitutions with two fluorines ($\Delta pK_a = -3.43$) and three fluorines ($\Delta pK_a = -4.26$) at this position increase the acidity.

Since a CF_3 group withdraws electrons only in an inductive manner, insertion of a methylene group between CF_3 and CO_2H moieties naturally diminishes its inductive effect.

Table 1.5 *Selected pK_a values of various fluorinated compounds [35, 59]*

Compound	pK_a	Compound	pK_a	Compound	pK_a
CH_3CO_2H	4.76	$CH_3CH_2CO_2H$	4.87	$(CH_3)_2CHOH$	17.1[a]
CH_2FCO_2H	2.59	$CF_3CH_2CO_2H$	3.06	$(CF_3)_2CHOH$	9.3[a]
CH_2ClCO_2H	2.87	$C_6H_5CO_2H$	4.21[a]	$(CH_3)_3COH$	19.0[a]
CH_2BrCO_2H	2.90	$C_6F_5CO_2H$	1.7[a]	$(CF_3)_3COH$	5.4[a]
CHF_2CO_2H	1.33	CH_3CH_2OH	15.93[a]	C_6H_5OH	9.99
CF_3CO_2H	0.50	CF_3CH_2OH	12.39[a]	C_6F_5OH	5.5[a]

[a] Ref. [59].

Nevertheless, the pK_a of 3,3,3-trifluoropropanoic acids is 3.06, which is still substantially more acidic than propanoic acid (pK_a = 4.87) (ΔpK_a = −1.81). Introduction of CF_3 groups to methanol dramatically increases the acidity of the resulting alcohols. Thus, pK_a values of CF_3CH_2OH, $(CF_3)_2CHOH$ and $(CF_3)_3COH$ are 12.39, 9.3 and 5.4, respectively. The pK_a value of $(CF_3)_3COH$ is only 0.7 larger than that of acetic acid.

As discussed above, the introduction of fluorine(s) to alkyl amines decreases their amine basicity, which results in higher bioavailability, in some cases, due to the increase in lipophilicity [60]. For example, the pK_a values of ethylamines decrease linearly upon successive fluorine introductions: $CH_3CH_2NH_2$ (10.7), $FCH_2CH_2NH_2$ (9.0), $F_2CHCH_2NH_2$ (7.3), and $F_3CCH_2NH_2$ (5.8) [58]. Based on experimental data, a practical method has been developed for the prediction of pK_a values of alkyl amines through the "σ-transmission effect" (i.e., inductive effect) of fluorine [58]. The inductive effects of fluorine and fluorine-containing groups confer favorable properties on some enzyme inhibitors. For example, a significant difference in potency was observed between $CF_3SO_2NH_2$ (pK_a = 5.8; $K_i = 2 \times 10^{-9}$ M) and $CH_3SO_2NH_2$ (pK_a = 10.5; K_i in 10^{-4} M range) for the inhibition of carbonic anhydrase II (a zinc metalloenzyme) [61, 62]. This can be attributed to the substantial increase in the acidity of the sulfonamide functionality by the introduction of a trifluoromethyl group, which facilitates deprotonation and better binding to the Zn(II) ion in the catalytic domain of the enzyme [61, 62].

Perfluorination of benzoic acid and phenol increases their acidity by 2.5 and 4.5 pK_a units, respectively (see Table 1.5). In these compounds, the π-electrons are localized at the center of the perfluorobenzene ring because of strong electronic repulsion between the lone pairs of five fluorines on the ring. When fluorine is bonded to an sp^2-hybridized carbon, a significant cationic charge distribution is observed at the carbon with fluorine (C^1), while a substantial negative charge develops at C^2 (see **10b** and **10c**), as shown in Figure 1.6 [*Note:* DFT computation was performed using Gaussian 03 (Revision B.03) by one of the authors (T.Y.)]. This remarkable polarization of a carbon–carbon double bond is attributed to the strong electronic repulsion between the π-electrons of the carbon–carbon double bond and the lone pairs of fluorine.

This phenomenon is unique to fluoroethenes (**10b** and **10c**) and the corresponding dichloroethene (**10d**) shows much weaker "p–π repulsion." This can be ascribed to the facts that (i) chlorine is a third-row element and its 3p lone pairs do not effectively interact with the $2p_z$ olefinic π-electrons, and (ii) the C–Cl bond is considerably longer than the C–F bond (1.744 Å for **10d** vs. 1.326 Å for **10c**, see also Table 1.1). Another unique structural feature of **10c** is its unusually small F–C^1–F bond angle (109.5°), which is 10.5°

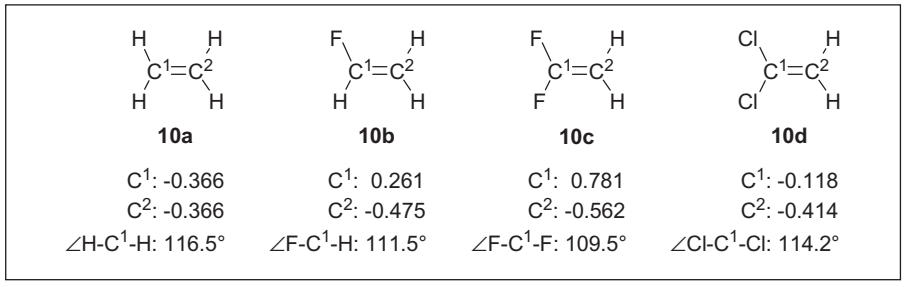

Figure 1.6 *Estimated charges on carbons in ethylenes,* ***10a-d****, by* ab initio *calculations.*

smaller than the angle expected for the ideal sp^2 hybridization [63, 64]. This might suggest a substantial contribution of an $F^{(+)}{=}C(F){-}^{(-)}CH_2$ resonance structure and an attractive electronic interaction between $F^{(+)}$ and F: [64].

1.1.5 Gauche Effect

The strong electronegativity of fluorine renders its related molecular orbitals relatively lower-lying. For example, a C–F bond can readily accept electrons to its vacant σ^*_{C-F} orbital from a vicinal electron-donating orbital, while the electron-occupied σ_{C-F} orbital is reluctant to donate electrons. Such characteristics often influence the three-dimensional shape of a molecule in a distinct manner. Figure 1.7 illustrates basic examples.

Two conformations, *gauche* and *anti*, are possible for 1,2-difluoroethane [14]. Based on the fact that fluorine is about 20% larger and much more electronegative than hydrogen, it is quite reasonable to assume that *anti***-14** should be more stable than *gauche***-14** from both steric and electrostatic points of view. However, this is not the case, and analyses by infrared spectroscopy [65], Raman spectroscopy [65], NMR [66] and electron diffraction [67, 68] have led to the unanimous conclusion that the latter conformation is preferred by approximately 1.0 kcal/mol, which was also confirmed by *ab initio* calculations [69, 70]. This phenomenon, termed the "*gauche effect*," is rationalized by taking into account stabilization through the critical donation of electrons from the neighboring σ_{C-H} orbital to the lower-lying vacant σ^*_{C-F} orbital as shown in Figure 1.7, which is not possible in the corresponding *anti* isomer. In the case of vicinal 1,2-dihaloethanes, this preference is observed specifically for 1,2-difluoroethane (**14**), because the increasing steric hindrance caused by two other halogens in the *gauche* geometry exceeds the energy gain by the orbital interaction using the energetically lowered $\sigma^*_{C-Halogen}$ [69, 70]. For example, an exchange of one fluorine in 1,2-difluoroethane (**14**) with chlorine (i.e., 1-fluoro-2-chloroethane) prefers the *anti* conformation on the basis of computational analysis as well as experimental results [71].

2-Fluoroethanol (**15**) also takes the *gauche* conformation predominantly [72–74]. Initially this preference was attributed to its possible formation of intramolecular *F*···*H*–O hydrogen bonding in addition to the *gauche* effect [72–74]. However, it was later found that 1-fluoro-2-methoxyethane, which could not form a hydrogen bond, also took the *gauche* conformation as its predominant structure [75, 76]. This finding clearly eliminated

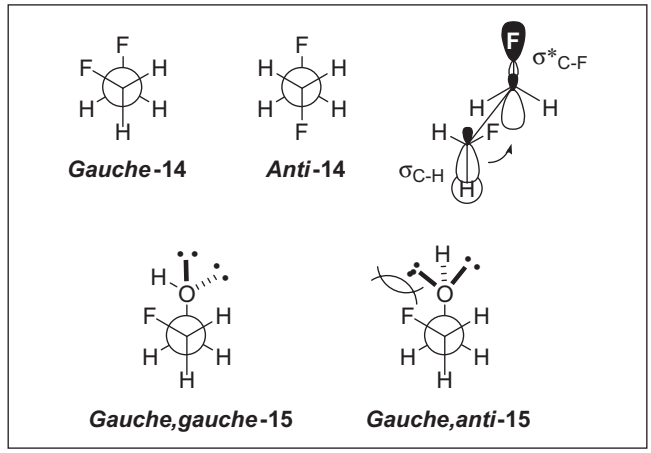

Figure 1.7 *Orbital interaction of 1,2-difluoroethane (**14**) and conformation of 2-fluoroethanol (**15**).*

the contribution of the *F···H*–O hydrogen bonding as the major reason for the dominant *gauche* conformation of **15** wherein the O–H is in parallel to the C–F bond. Thus, it is most likely that **15** takes this particular conformation to minimize unfavorable electronic repulsion between the lone pairs of the oxygen and fluorine [75]. The absence of *F···H*–O and *F···H–N* hydrogen bonding was also confirmed for α-fluorocarboxamides [77] and 2-fluoroethyl trichloroacetate [78].

It has been shown that the *gauche* effect plays a key role in controlling the conformation of various acyclic compounds [79]. For example, the x-ray crystallographic analysis of difluorinated succinamides, *syn*-**16** and *anti*-**16** shows unambiguously that these compounds take *gauche* conformation with *F*–C–C–*F* dihedral angles of 49.0° and 75.2°, respectively (see Figure 1.8). *Syn*-**16** and *anti*-**16** possess respectively two and one $\sigma_{C-H}\cdots\sigma^*_{C-F}$ interactions which are reflected in the lengths of their (F)*C*–*C*(F) bonds: 1.495 Å and 1.538 Å, respectively, the former being 0.043 Å shorter than the latter (see Figure 1.7). Although the conformation of *syn*-**16** might look reasonable by taking into account the *antiperiplanar* placement of two bulky amide moieties, it is not the case for *anti*-**16**, indicating the importance of the *gauche effect*. In the latter case, however, a 7-membered ring hydrogen bond between two amide groups might also make some contribution. Similar *gauche* effects have been reported in other systems [80–84].

The *gauche* effect is also clearly observed in the conformational preference of 4-fluoroprolines (**17b** and **17c**) determined by ^{1}H NMR analysis [85]. As Table 1.6 shows, (4*R*)-fluoroproline (**17b**: R^1 = F, R^2 = H) strongly prefers the C$^\gamma$-*exo* conformation in which an electron-releasing C$^\gamma$–H bond should occupy the antiperiplanar position to the electron-accepting C–F group to maximize the *gauche* effect. On the other hand, its epimer (4*S*)-fluoroproline (**17c**: R^1 = H, R^2 = F) takes the C$^\gamma$-*endo* conformation almost exclusively to optimize the $\sigma_{C-H}\cdots\sigma^*_{C-F}$ interaction for the *gauche* effect. It should be noted that the observed preferences are independent of the *trans* or *cis* amide linkage by calculation [85].

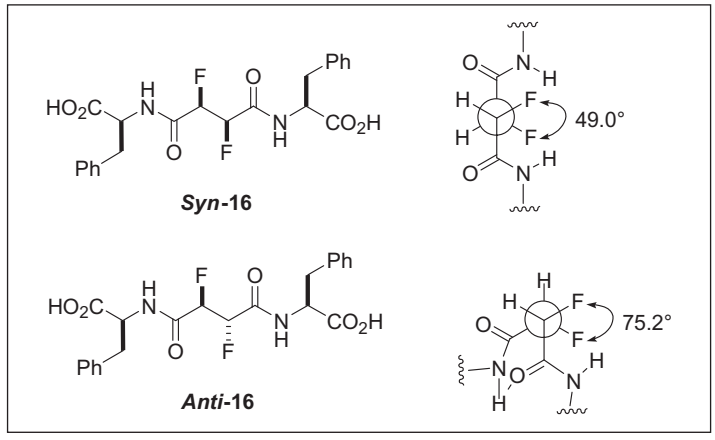

Figure 1.8 *Conformation of diastereomeric* ***16*** *by X-ray crystallographic analysis.*

Table 1.6 *Conformational preference of Ac-Xaa-OMe (Xaa = proline and its derivative) [85]*

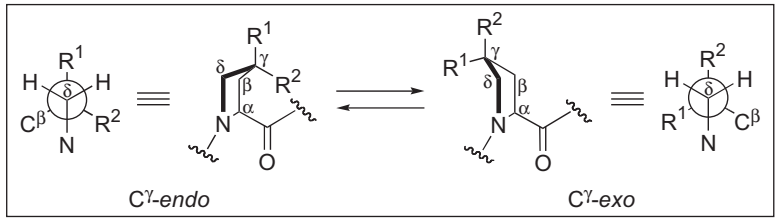

Xaa in Ac-Xaa-OMe	R^1	R^2	Conformation			$\Delta E_{endo} - E_{exo}$ (kcal/mol)	
			endo	:	*exo*	*trans*	*cis*
Proline (**17a**)	H	H	66	:	34	–0.41	–0.60
(4*R*)-4-Fluoroproline (**17b**)	F	H	14	:	86	0.85	1.18
(4*S*)-4-Fluoroproline (**17c**)	H	F	95	:	5	–0.61	–1.99

1.1.5.1 Unique Electronic Effects of Fluorine Related to the Origin of the Gauche Effect

The interaction of the σ^*_{C-F} orbital with the lone pairs of fluorine in fluorinated methanes is substantial [83]. In these compounds, the C–H bond length is almost constant regardless of the number of fluorines in a molecule. In sharp contrast, the C–F bond length decreases as the number of fluorines increases due to substantial n_F–σ^*_{C-F} interaction mentioned above [83]. Alternatively, a significantly strong positive charge developed on carbon may play a key role in strengthening C–F bonds in an electrostatic manner [82].

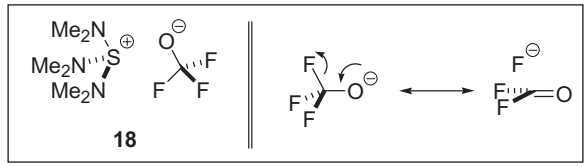

Figure 1.9 *Compound **18** and negative hyperconjugation in CF_3–O^- anion.*

"Negative hyperconjugation" of fluorine [86–89], essentially the same electron donation pattern as that of the *gauche* effect, that is, interaction of an electron-rich bond with the lower-lying vacant orbital of a polarized neighboring C–F bond (σ^*_{C-F}), has been clearly observed in the X-ray structure of $[(CH_3)_2N]_3S^+CF_3O^-$ (**18**) (see Figure 1.9) [90]. The counter-anion, CF_3O^-, of **18** possesses a significantly short C–O bond (1.227 Å) and long C–F bonds (1.390 and 1.397 Å). For comparison, the gas-phase structures of electronically neutral counterparts, CF_3OR (R = F, Cl, CF_3), show 1.365–1.395 Å and 1.319–1.327 Å for the C–O and C–F distances, respectively [90]. It is worthy of note that the C–O single bond length in CF_3O^- (1.227 Å) is close to that of a C=O bond length (e.g., 1.171 Å for $F_2C{=}O$) and the F–C–F bond angle is extraordinarily small (101.7° and 102.2°) compared with the ideal sp^3 bond angle (109.5°). This phenomenon strongly indicates the effective orbital interaction of the electron rich n_O orbital with lower-lying σ^*_{C-F} orbital, i.e., negative hyperconjugation.

1.1.6 Hydrogen Bonding

Fluorine can share three sets of lone-pair electrons with electron-deficient atoms intramolecularly or intermolecularly, in particular with a relatively acidic hydrogen bound to a heteroatom. In addition, as described in section 1.4, strongly electron-withdrawing perfluoroalkyl groups increase the acidity of proximate functional groups such as alcohol, amine, amide, and carboxylic acid.

It is readily anticipated that the acidity of CF_3-containing benzylic alcohol **19** is as high as or higher than that of phenol (see Table 1.5 for hexafluoro-2-propanol). Moreover, a fluorine atom of the CF_3 groups at the 3- and 5-positions should increase its anionic character by negative hyperconjugation (see above). Thus, it is reasonable to assume that the benzylic hydroxyl group would form a hydrogen bond with a proximate CF_3 group [91, 92]. In fact, the X-ray crystallographic analysis of **19** shows that **19** forms a unique dimer structure in the solid state through two strong intermolecular hydrogen bonds (H···F distance is 2.01 Å), as illustrated in Figure 1.10 [91]. The strength of this hydrogen bond is obvious by comparing the sum of the van der Waals radii of H and F (2.67 Å) with the observed H···F bond length (2.01 Å). On the other hand, **19** appears to form an intramolecular hydrogen bonding between the same benzylic hydroxyl CF_3 groups in a hexane solution on the basis of low-temperature ^{13}C NMR analysis, as illustrated in Figure 1.10. Although the *C*F_3 carbon appeared as a normal quartet (J_{C-F} = 274 Hz) at 24 °C, the coupling pattern was changed to the doublet of triplet (J_{C-F} = 261, 279 Hz, respectively) at –96 °C. The result appears to indicate the nonequivalence of three fluorine atoms in the CF_3 groups, and only one of the three fluorine atoms participates in the hydrogen bonding.

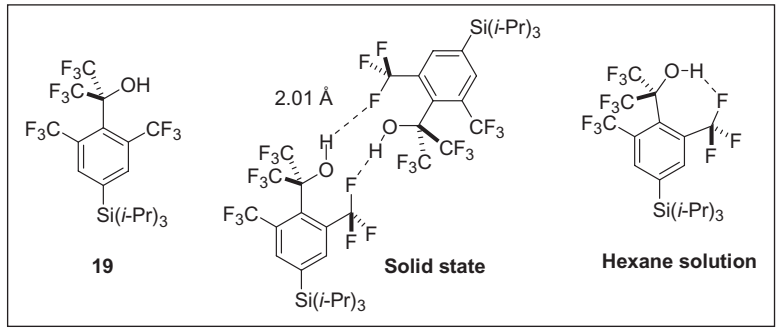

Figure 1.10 *Intermolecular and intramolecular H···F hydrogen bonding patterns of* ***19****.*

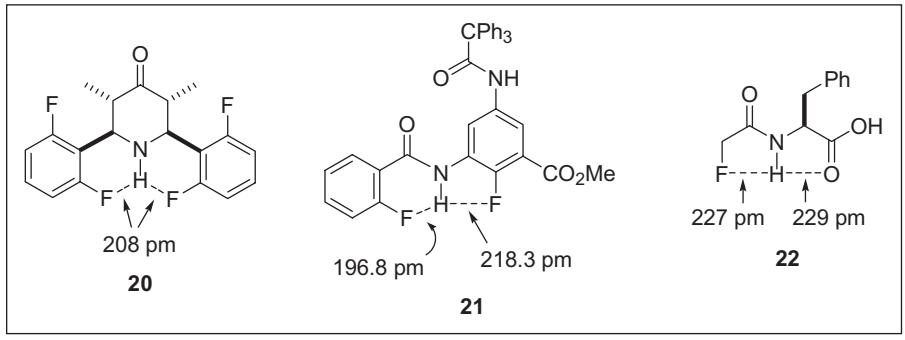

Figure 1.11 *Representative intramolecular NH···F hydrogen-bonding interactions.*

However, very recently, a counterargument on this hydrogen bonding suggested that the nonequivalence of three fluorine atoms of the CF_3 groups should be attributed to steric crowding and not H–F hydrogen bonding [93]. Accordingly, the interpretation of the NMR data is still unsettled.

Similar hydrogen bonding has been observed between fluorine and amine or amide hydrogen. The NH···F hydrogen bond is especially favorable with an amide hydrogen because of its acidity compared with that of an amine. Figure 1.11 illustrates three representative compounds, **20**, **21**, and **22** whose structures were determined by X-ray crystallography. The H···F distance of **20** is 2.08 Å, which is 0.59 Å shorter than the sum of the van der Waals radii [94]. Compound **21** includes two hydrogen bonds with six- and five-membered ring systems, bearing NH···F distances 1.97 Å and 2.18 Å, respectively [95]. The NH moiety of *N*-fluoroacetylphenylalanine (**22**) also formed a bifurcated intramolecular hydrogen bonds with F and O with practically the same bond lengths: 2.27 Å and 2.29 Å, respectively [96].

Fluorinated benzenes, in general, have been shown to form intermolecular hydrogen bonds in the solid state. Among those fluorobenzenes, the X-ray crystal structure of 1,2,4,5-tetrafluorobenzene (**24**) exhibited the shortest intermolecular H···F distance of

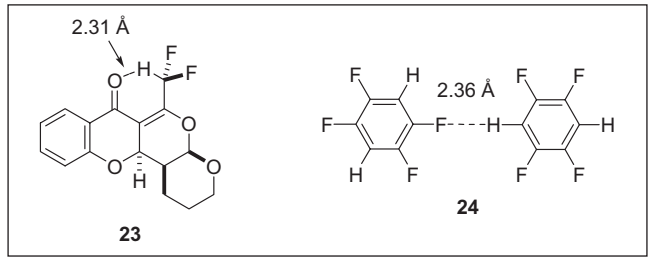

Figure 1.12 *Other hydrogen-bonding patterns.*

2.36 Å [97] (see Figure 1.12). Although it is not H···F bonding, a related hydrogen bonding pattern has been reported. As Figure 1.12 illustrates, the X-ray crystallographic analysis of chromone **23** shows the *O*···*H*–CF_2 distance of 2.31 Å (the sum of the van der Waals radii of H and O is 2.72 Å) [98, 99]. Other C=*O*···*H*–CF_2 bonding examples have been reported [100].

1.1.7 Orthogonal multipolar C–F Bond–Protein Interactions

It has recently been shown that polar C–F bond–protein interactions play a critical role in the stabilization of fluorine-containing drugs and their target proteins [101]. These polar interactions are found in the X-ray crystal structures of drug-protein complexes compiled in the Cambridge Structural Database (CSD) and the Protein Data Bank (PDB) [20–32, 101]. A large number of examples for the polar C–F bond–protein interactions, found in the CSD and PDB through database mining, include those between a C–F bond and polar functional groups such as carbonyl and guanidinium ion moieties in the protein side chains, that is, C–*F*···*C*=O and *C*–*F*···C(NH_2)(=NH). The majority of examples from the protein crystallographic database indicate that a C–F bond unit serves as a poor hydrogen-bond acceptor. Instead of hydrogen bonding, however, a C–F bond forms polar interactions with a large number of polarizable bonds in the manner as C–F···X(H) (X = O, N, S) and C–F···C_α–H (C_α = α-carbon of the α-amino acid), in which the F···H–X separation is well beyond hydrogen-bonded contact distance [101].

For example, a thrombin inhibitor **25** (K_i = 0.25 μM) is more potent than the nonfluorinated counterpart (K_i = 1.6 μM) and the X-ray crystal structure of the inhibitor–enzyme complexes showed remarkable conformational differences between the two inhibitors. This conformational change is caused by the dipolar C–F···N(H)(Gly216) interaction with a F–N distance of 3.5 Å, as illustrated in Figure 1.13a [25].

A large number of examples for the orthogonal dipolar C–F···C=O interactions have been found in the CSD and PDB [101]. For example, Figure 1.13b illustrates a rather unique double interaction, that is, C–F···$(C=O)_2$, in the inhibitor–enzyme complex of **26** with p38 MAP kinase, wherein the fluorine atom of the 4-fluorophenyl moiety of **26** interacts with the amide carbonyl carbons of Leu104 and Val105 with equal distance of 3.1 Å [102].

Table 1.7 summarizes systematic SAR studies of tricyclic thrombin inhibitors, *rac*-**27** and *rac*-**28**, through "fluorine scan" to map the effects of fluorine introduction on

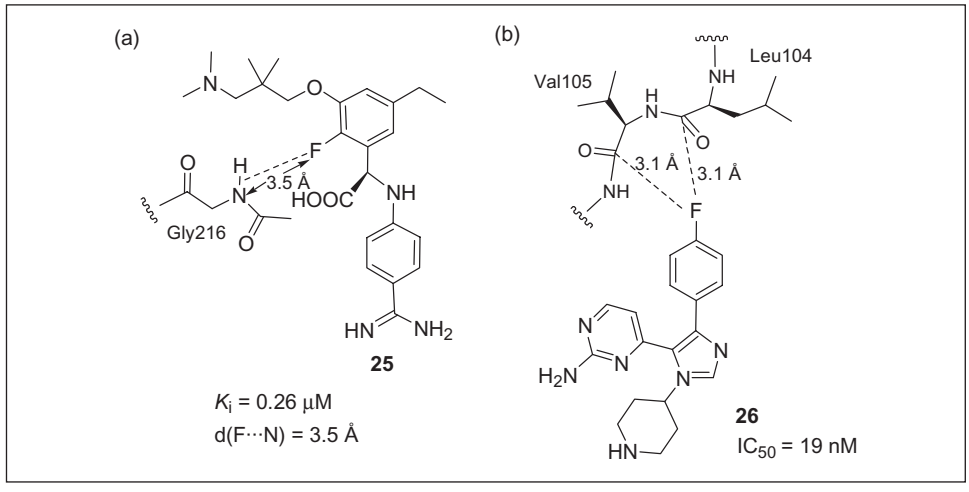

Figure 1.13 *(a) Interaction of C–F···N(H)(Gly216) in the thrombin-inhibitor* ***25*** *complex. (b) C–F···C=O multipolar interactions of p38 MAP kinase inhibitor* ***26*** *with the kinase.*

Table 1.7 *Enzyme inhibitory activity of tricyclic thrombin inhibitors [105]*

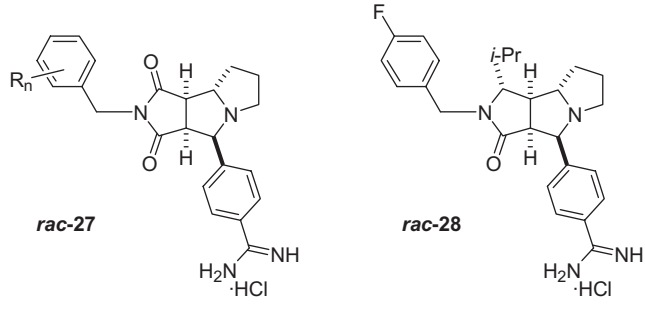

Inhibitor	Substituent[a]	K_i[b] (mM)	Selectivity[c]	log *D*
27a	–	0.31	15	–1.24
27b	2-F	0.50	9.8	<–1.00
27c	3-F	0.36	26	–1.24
27d	4-F	0.057	67	–1.08
27e	2,3-F_2	0.49	18	–[d]
27f	2,6-F_2	0.61	9.0	–[d]
27g	3,4-F_2	0.26	29	–[d]
27h	3,5-F_2	0.59	25	–1.25
27i	2,3,4,5,6-F_5	0.27	44	–1.14
27j	4-Cl	0.19	30	–[d]
28	4-F	0.005	413	–[d]

[a] Substituents on the benzene ring of the benzylimide moiety.
[b] With ±20% uncertainty.
[c] K_i (trypsin)/K_i (thrombin).
[d] Not determined.

inhibitory activity, change of amine basicity, and favorable interactions of C–F bonds with the protein [103–106].

Inhibitory activity, selectivity between thrombin and trypsin and lipophilicity (log *D*) of *rac*-**27** are shown in Table 1.7, which indicates that 4-monofluorinated analog *rac*-**27d** is the most potent inhibitor in this group (K_i = 0.057 mM; K_i(trypsin)/K_i(thrombin) selectivity = 67) [105]. The inhibitory activity K_i is further optimized to 5 nM by changing the imide ring of *rac*-**27** to a lactam bearing an isopropyl group, *rac*-**28**, wherein the isopropyl group fits better in the P-pocket (see Figure 1.14). The trypsin/thrombin selectivity of *rac*-**28** is also dramatically improved to 413 [105].

The X-ray crystallographic analysis of the enantiopure **27d**–thrombin complex indicates that the H–C_α–C=O fragment of the Asn98 residue possesses significant "fluorophilicity" [105]. As Figure 1.14 illustrates, the C–F residue of enantiopure **27d** has strong multipolar C–F···C_α–H [d(F–C_α) = 3.1 Å] and C–F···C=O [d(F–C=O) = 3.5 Å] interactions with the Asn98 residue in the distal hydrophobic pocket ("D pocket") of thrombin. It is worthy of note that the C–F bond and the electrophilic carbonyl group are positioned in a nearly orthogonal manner along the pseudotrigonal axis of the carbonyl group [105]. This preferred geometry for the C–F···C=O interactions is further corroborated by the X-ray crystal structure analyses of fluorine-containing small molecules [103–106] and the database mining of PDB and CSD [107–110]. The latter furnished numerous cases

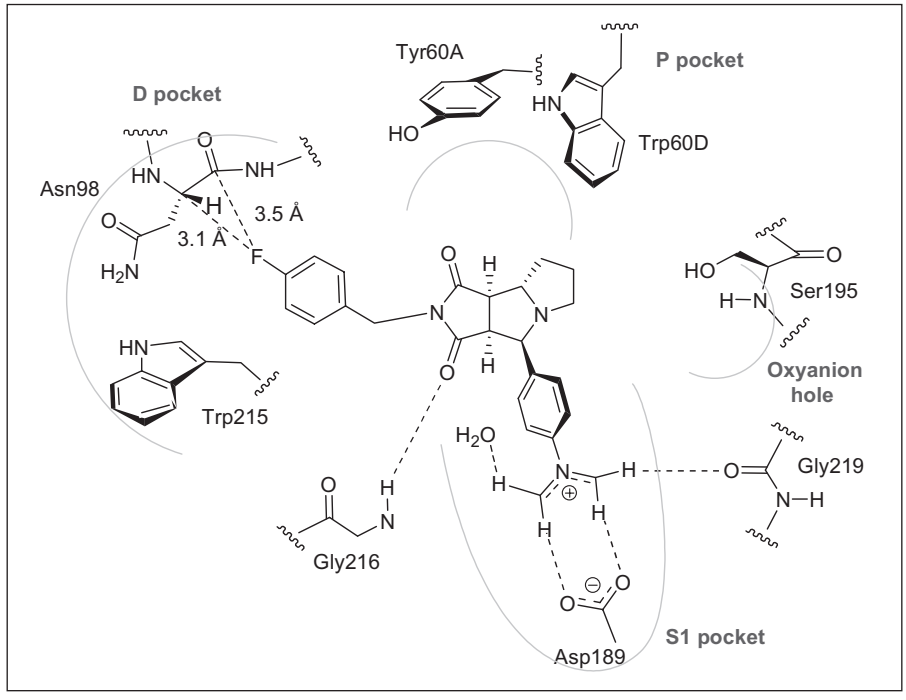

Figure 1.14 *Binding mode of tricyclic thrombin inhibitor* ***27d*** *on the basis of X-ray crystallographic analysis of its protein complex.*

of C–F···C=O contacts with the F···C distance below the sum of the van der Waals radii and the C–F···C=O torsion angle toward 90°. A similar but intramolecular orthogonal polar interaction between a CF_3 groups and a spatially close amide C=O group, which plays a role in the folding of an extended indole molecule, has recently been reported [111].

Figure 1.15 illustrates an example of the polar interaction of a C–F bond with the guanidinium carbon of the Arg residue in an enzyme, revealed by the X-ray crystal structure of atorvastatin-HMG-CoA reductase (HMG-CoA = 3-hydroxy-3-methylglutaryl-coenzyme A; the rate-determining enzyme in the biosynthesis of cholesterol). As mentioned above (see section 1.1), atorvastatin is the best-selling cholesterol-lowering drug, which binds to HMG-CoA reductase tightly (IC_{50} = 8 nM). In the early stage of the drug discovery, a series of phenylpyrrole-hydroxylactones were evaluated for their inhibitory activity against HMG-CoA reductase, as shown in Figure 1.15a. Then, the SAR study on the 4-substituted phenyl analogues identified that the 4-fluorophenyl analogue (R = F) was the most active; that is, fluorine was better than hydrogen, hydroxyl or methoxy group at this position [112]. This finding eventually led to the discovery of atorvastatin. The X-ray crystal structure of atorvastatin–HMG-CoA reductase [113] shows a strong C–F···C(NH_2)(=NH) polar interaction between the 4-fluorophenyl moiety and the Arg590 residue of the enzyme with a very short F···C distance (2.9 Å), as illustrated in Figure 1.15b [101].

Several other examples of similar polar interactions between a C–F bond in a ligand and the guanidinium ion moiety of an Arg residue in protein have been found in PDB. However, no linear C–F···H–N interactions are identified, reflecting the poor hydrogen-bond accepting ability of a C–F bond. Instead of hydrogen bonding, a C–F bond is found to orient either parallel or orthogonal to the plane of the guanidinium ion moiety, bearing a delocalized positive charge. These examples confirm the fluorophilic character of the guanidinyl side-chain of an Arg residue.

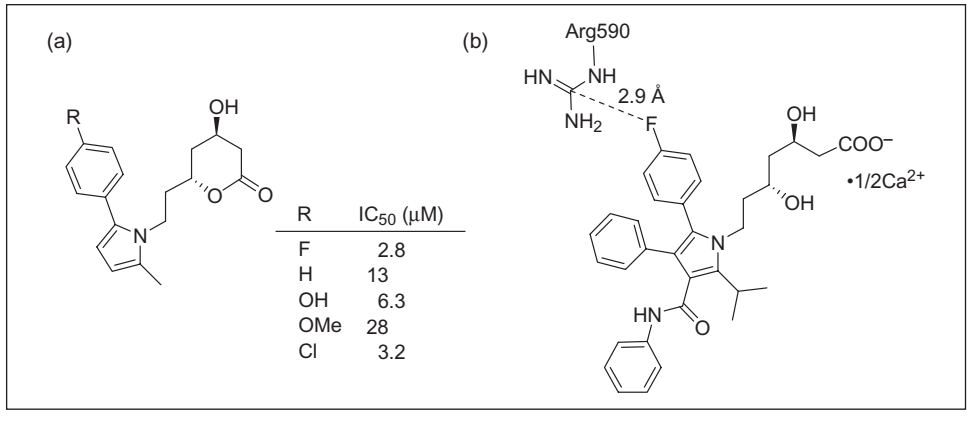

Figure 1.15 *(a)* In vitro *activity of HMG-CoA reductase inhibitors. (b) Orthogonal polar interaction of the fluorine substituent of atorvastatin with Arg590 in HMG-CoA reductase.*

1.1.8 Isostere

A variety of natural and synthetic peptides exhibit biological activities, which can be developed as pharmaceutical drugs or biochemical agents. However, those peptides consisting of amide linkages are, in most cases, easily deactivated through cleavage of key amide bonds by hydrolytic enzymes. Accordingly, it is very useful if a key amide bond is replaced with noncleavable bond, keeping the characteristics of the amide functionality.

An amide linkage in a peptide such as **29a** has an imidate-like zwitterioninc resonance structure **29b**. Since the contribution of this resonance structure is significant, free rotation around the C–N bond is partially restricted because of the substantial double-bond character of the C–N bond (see Figure 1.16). Accordingly, it might be possible to replace an amide linkage with its isostere (i.e., a molecule having the same number of atoms as well as valence electrons [114]), regarded as a "peptide isostere."

The first and simplest attempt at the "peptide isostere" was made by replacing an amide bond of enkephalin with a *trans*-olefin unit [115], but it did not give a desirable effect. However, computational analysis of a model amide, *N*-methylacetamide (**30b**) and its isosteres, by semiempirical molecular orbital calculation revealed that fluoroolefin **30c** resembled **30a** much more closely than **30b** [116]. To confirm this finding based on a semiempirical method, the *ab initio* analysis of **30a**, (*E*)-2-butene (**30b**), (*Z*)-2-fluoro-2-butene (**30c**) and (*Z*)-1,1,1-trifluoro- 2-methyl-2-butene (**30d**) was carried out using the Gaussian 03 program (B3LYP/6–311++G**) [117] by one of the authors (T. Y.), which gave electrostatic potentials of these compounds. The results are illustrated in Figure 1.17.

As readily anticipated, **30a** has a very negative oxygen, a highly positive carbonyl carbon, a highly negative nitrogen, and a very positive NH hydrogen. In sharp contrast, **30b** has a nonpolarized negative C=C bond and only weakly positive CH hydrogen. Thus, it is apparent that **30b** does not mimic **30a** electronically. In contrast, **30c** has an appropriately polarized C=C double bond, a negative fluorine atom in place of the oxygen atom of amide **30a**, and a positive CH in place of the NH moiety of amide **30a**. Thus, **30b** indeed mimics **30a** electronically. Finally, **30d** has a nonpolarized C=C bond, a modestly positive CH hydrogen, and three negative fluorine atoms. Thus, **30d** mimics **30a** electronically to some extent, although sterically the CF_3 group is much bulkier than an oxygen atom.

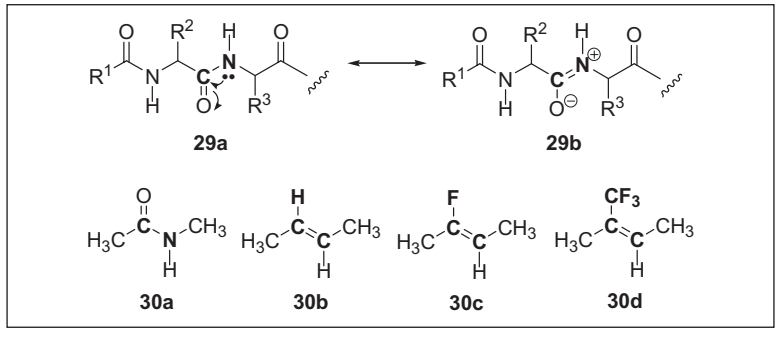

Figure 1.16 *Resonance structures of amide **29**, amide **30a**, and its isosteres **30b–d**.*

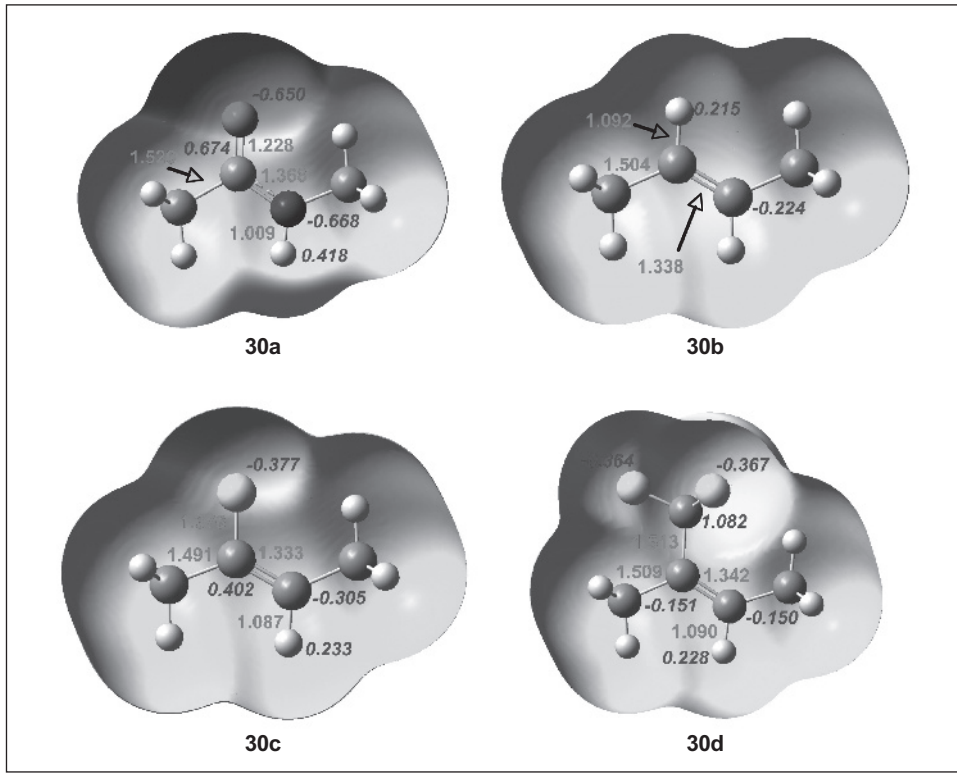

Figure 1.17 *Electrostatic potential of the model compounds* ***30a*** *to* ***30d*** *(color alteration from red to blue describes the shift of the electronically rich to deficient circumstance). See color plate 1.17.*

A fluoroolefin isostere was successfully introduced to a physiologically important neuropeptide, Substance P (**31**) [118]. As Figure 1.18 shows, the (*E*)-fluoroethene isostere replaced the peptide linkage between the Phe[8]-Gly[9] residues of **31** to give Substance P analogue **32a** and its epimer **32b** [119]. The neurokinin-1 receptor binding assay of **32a** disclosed that **32a** was almost as potent as the original peptide **31**. On the other hand, its epimer **32b** was 10 times less potent than **32a**, as anticipated.

Another fluoroolefin isostere, (*E*)-trifluoromethylethene, was also introduced to antibiotic Gramicidin S (**33a**), replacing the peptide linkage between Leu and Phe (two sites) to give an analogue **33b**, as illustrated in Figure 1.19 [120]. Variable-temperature NMR measurements of **33a** and **33b** indicated that the NH(Leu) and NH(Val) protons were forming intramolecular hydrogen bonds. In addition, NOESY experiments of **33a** and **33b** showed interstrand NOEs between NH(Leu) and NH(Val) as well as NH(Leu) and H_{α}(Orn) in both compounds. Moreover, X-ray crystallographic analysis of **33c** confirmed the presence of a pair of intramolecular hydrogen bonds between NH(Leu) and C=O(Val) (1.96 Å and 2.00 Å). However, the replacement of the Leu-Phe amide linkage with the bulky (*E*)-trifluoromethylethene isostere caused a 70° twist in the plane of the C=C double bond

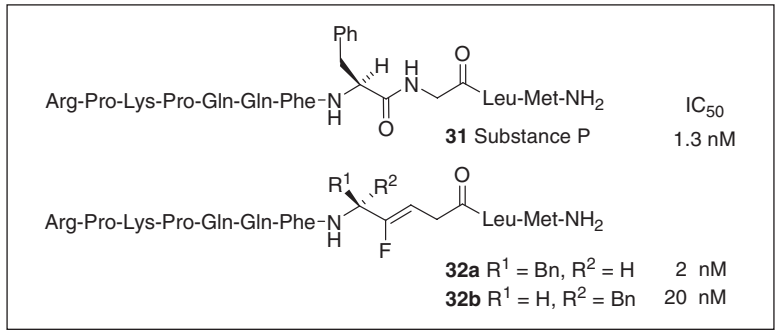

Figure 1.18 *Substance P (**31**) and its fluoroolefin dipeptide isosteres (**32a, b**).*

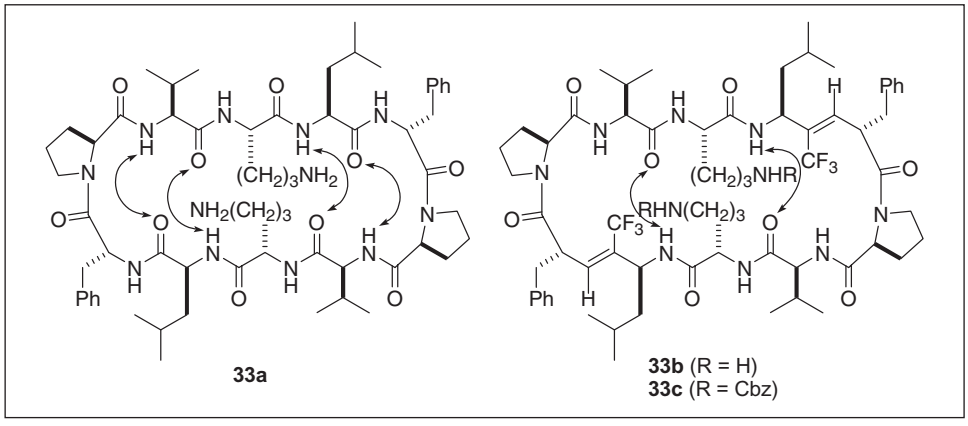

Figure 1.19 *Gramicidin S (**33a**) and its CF_3-containing isostere (**33b**).*

compared with the amide moiety in the original β-turn structure of **33a**. This is very likely attributable to the bulkiness of the CF_3 groups, which are difficult to be accommodated inside the β-turn hairpin structure. In spite of some conformational difference, **33b** was found to possess high antibiotic activity against *Bacillus subtilis* equivalent to that of **33a** [120]. The use of the (*E*)-trifluoromethylethene peptide isostere as β-turn promoter and peptide mimetics in general has also been studied [121]. A fairly large dipole moment of this isostere ($\mu = 2.3$ D) appears to play a key role in the improved mimicry of the electrostatic potential surface of the amide linkage (dipole moment of the amide unit: $\mu = 3.6$ D) [120].

Although fluoroethene and trifluoroethene peptide isosteres were successfully employed as nonhydrolyzable amide substitutes, more recently trifluoroethylamines have emerged as highly promising peptide isosteres. The trifluoroethylamine isostere has been studied for partially modified retro- and retro-inverso Ψ[NHCH(CF_3)]Gly peptides [122, 123]. Furthermore, it has been demonstrated that the CF_3 group of the trifluoroethylamine

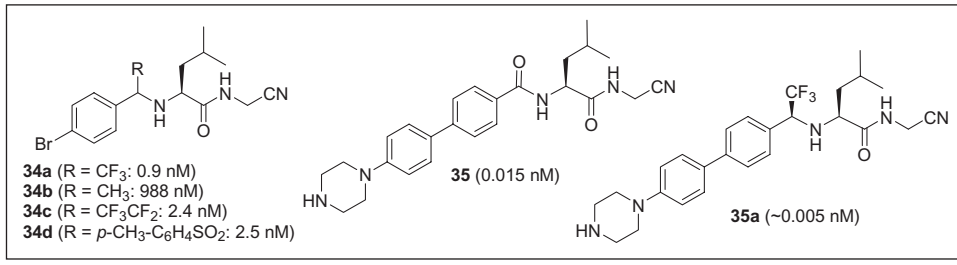

Figure 1.20 *Cathepsin K inhibitors **34** and **35**, bearing trifluoroethylamine isosteres. Numbers in parentheses are IC_{50} values.*

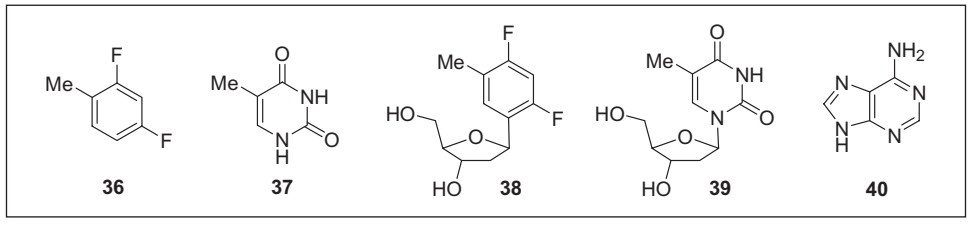

Figure 1.21 *Difluorotoluene (**36**), difluorotoluene deoxyriboside (**38**), thymine (**37**), thymidine (**39**) and adenine (**40**).*

isostere can function as the carbonyl group of an amide to provide a metabolically stable, nonbasic amine that has excellent hydrogen-bonding capability due to the strong inductive effect of the CF_3 group [124, 125]. These unique characteristics of the trifluoroethylamine isostere have been exploited and quite successfully applied to the optimization of cathepsin K inhibitors, which are promising antiresorptive agents for treatment of osteoporosis [124]. As Figure 1.20 shows, trifluoroethylamine analogue **34a** exhibits 1000 time better potency than the corresponding ethylamine analogue **34b**. Pentafluoroethylamine analogue **34c** possesses a somewhat reduced activity, but still in a comparable level to **34a**. Tosylmethylamine analogue **34d** shows virtually the same activity as that of **34c**. The docking study using the cathepsin K crystal structure has revealed that **34a** forms a critical hydrogen bond with the carbonyl oxygen of Gly66, as anticipated. The fact that the CF_3 group of this isostere is attached to an sp^3 carbon provides flexibility in the orientation of the NH bond to form hydrogen bonding in the most favorable manner [124]. Optimization of the aromatic group of **34a** led to the discovery of the exceptionally potent inhibitor **35a**, exhibiting an IC_{50} of 5 pM or less. The corresponding amide **35** is also extremely potent (IC_{50} = 0.015 nM) but is metabolically labile. Thus, **35a** has been identified as the most potent and promising drug candidate in this study [124].

It has been shown that 2,3-difluorotoluene (**36**) serves as a nonpolar shape mimic of thymine (**37**) and difluorotoluene deoxyriboside (**38**) is, surprisingly, an excellent nonpolar nucleoside isostere of thymidine (**39**) (see Fig. 1.21) [126, 127]. Thus, the nucleotide of **36** was incorporated into DNA by several high-fidelity DNA polymerases [126, 128],

forming a positional pair with adenine (**40**) in place of **37** without perturbing the double helix structure, which was confirmed by X-ray crystallography (see Fig. 1.21) [127]. It has also been shown that difluorotoluene does not form appreciable hydrogen bonds with adenine, and hence it is nonselective in base pairing and destabilizing DNA *in the absence of* DNA polymerases [128]. The probability of thymidine triphosphate choosing a wrong partner is less than 0.1% and that of the triphosphate of **38** is less than 0.3% [126]. Thus, the results clearly indicate that **36** is virtually a perfect shape mimic of **37** for DNA polymerases.

Since these surprising findings, first made in 1997, challenge the Watson–Click base-pairing principle in DNA (although the difluorotoluene isostere is only a minor part of DNA), there has been a debate on the interpretation of the results, including the polarity of **36** and possible F···HN as well as CH···N hydrogen bonding interactions [129]. However, the X-ray crystallographic data [127] as well as extensive computational analysis [130] unambiguously confirmed that **36** is indeed a nonpolar thymine isostere. Thus, these findings have opened a new avenue of research on a variety of nonpolar nucleoside isosteres [128].

1.1.9 Difluoromethylene as Isopolar Mimic of the Oxygen Component of P–O–C Linkage

Difluoromethylene has been recognized as an isopolar mimic of the oxygen component of P–O–C or P–O–P linkage in phosphates, which can be used to generate nonhydrolyzable phosphate analogues of nucleotides, enzyme substrates, and enzyme inhibitors [131–137]. For example, a difluoromethylene linkage was successfully introduced to a protein-tyrosine phosphatase (PTP) inhibitor of insulin receptor dephosphorylation [132] (see Figure 1.22). A comparison of a hexamer peptide inhibitor bearing a phosphonomethylphenylalanine (Pmp) residue (**41a**) with that having a phosphonodifluoromethylphenylalanine (F_2Pmp) residue (**41b**) revealed that **41b** was 1000 times more potent than **41a**, retaining high affinity for the SH2 domain of PTP [132]. The marked difference in potency observed for **41a** and **41b** can be ascribed to the fact that the difluoromethylene group increases the acidity of the phosphonic acid moiety and maintains appropriate polarity.

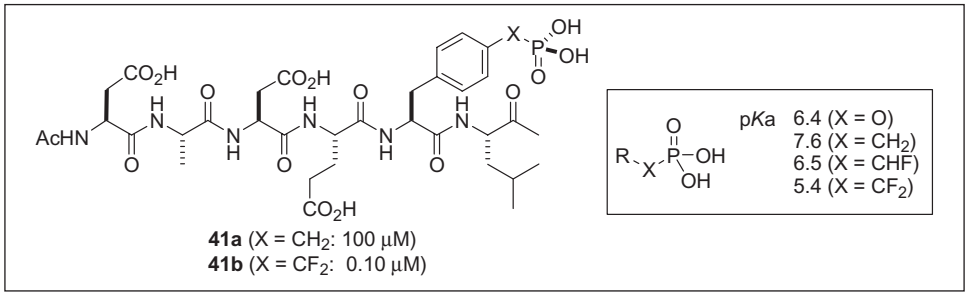

Figure 1.22 *Nonhydrolyzable phosphate mimics **41** and their estimated pKa values. Numbers within the parentheses are IC_{50} values.*

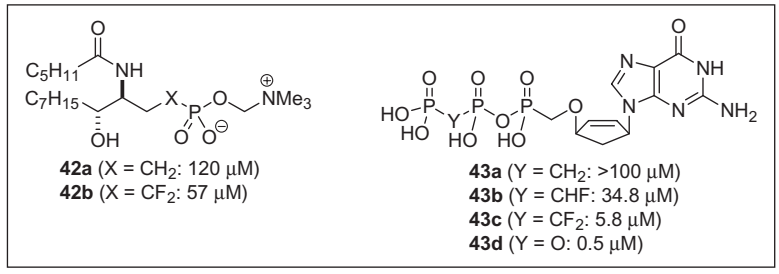

Figure 1.23 *SMase inhibitors (**42**) and FKBP 12 rotamase inhibitors (**43**). Numbers within the parentheses are IC_{50} values.*

A similar incorporation of a P–CF_2 unit as a P–O bond surrogate to sphingomyelin was reported [134] for the development of nonhydrolyzable inhibitors of sphingomyelinase (SMase), which cleaves sphingomyelin to release ceramide. As Figure 1.23 shows, difluoromethylene analogue **42b** is twice as potent as methylene analogue **42a** in the inhibition of SMase from *B. cereus* [134].

Norcarbovir triphosphate (**43d**) is a potent inhibitor of HIV reverse transcriptase, comparable to AZT and carvovir, but is amenable to enzymatic hydrolysis *in vivo* [135]. Thus, methylenediphosphonate, fluoromethylenediphosphonate, and difluoromethylenediphosphonate analogues of **43d** were synthesized to block the enzymatic hydrolysis and evaluated for their potency and stability in human fetal blood serum [135]. As Figure 1.23 shows, the methylenediphosphonate analogue (**43a**) is inactive, and the fluoromethylenediphosphonate analogue (**43b**) shows only a moderate potency. Difluoromethylenediphosphonate analogue **43c** is the most active among these nonhydrolyzable analogues with IC_{50} of 5.8 μM, which is 10 times weaker than that of **43d**. Nevertheless, **43c** possesses >40 times longer half-life (45 h) than the natural enantiomer of **43d** (65 min) and >500 times more stable than AZT triphosphate (5 min) [135].

The fluoromethylene and difluoromethylene linkages have also been incorporated into an aspartyl phosphate, providing the first synthetic inhibitors of aspartate semialdehyde dehydrogenase [136] as well as lysophosphatidic acid analogues, which increased the half-lives of analogues in cell culture [137].

The use of a difluoromethylene unit as a surrogate of a carbonyl group is another logical extension. In fact, difluoromethylene analogues of the inhibitors of the rotamase activity of FK506 binding protein 12 (FKBP12), which catalyzes *cis–trans* isomerization of a peptidyl-prolyl bond, have been investigated [138]. As Table 1.8 shows, the K_i values of difluoromethylene analogues, **44a** and **44d**, for the FKBP12 inhibition (rotamase activity) are comparable to or better than those of the carbonyl counterparts, **44b** and **44e**. It should be noted that the corresponding simple methylene analogues, **44c** and **44f** do not show any appreciable activity, which suggests that the *gem*-difluoromethylene group participates in some specific interactions with the protein. After optimization of the proline and its ester moieties, the most potent inhibitor **45** (K_i 19 nM) was developed. The X-ray crystal structure of the **45**–FKBP12 complex strongly suggests that the two fluorine atoms participate in the moderate-to-weak hydrogen bonding interactions with the Phe36 phenyl ring as well as Tyr26 hydroxyl group.

Table 1.8 *FKBP12 rotamase inhibition [138]*

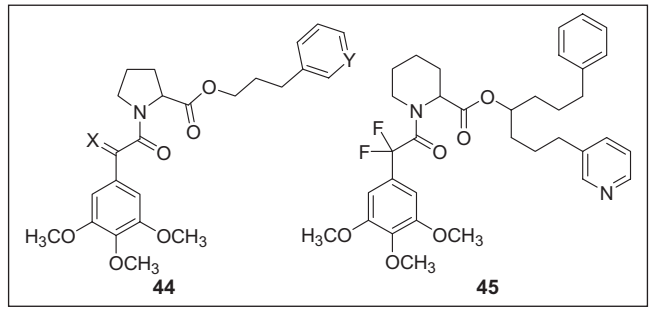

Compound	X	Y	K_i (μM)
44a	F_2	N	0.872
44b	O	N	4.00
44c	H_2	N	–[a]
44d	F_2	CH	1.30
44e	O	CH	2.20
44f	H_2	CH	–[a]
45			0.019

[a] No appreciable inhibition at 10 μM.

1.1.10 High Electrophilicity of Fluoroalkyl Carbonyl Moieties

Successive substitution of hydrogen atoms in acetone with fluorine atoms clearly lowers the frontier orbital energy levels by 0.2–0.6 eV on the basis of *ab initio* computation (see Table 1.9). It is worthy of note that the positive charge at the carbonyl carbon and the negative charge at the oxygen atoms in these ketones, *decrease* as the number of fluorine atoms increases. The validity of the computational analysis is confirmed experimentally by the ^{13}C NMR chemical shifts of these carbons, which decrease from 206.58 ppm for acetone to 172.83 ppm for hexafluoroacetone, in good agreement with the carbonyl carbon charges, as shown in Table 1.9.

The substantial decrease in the HOMO (highest occupied molecular orbital) energy level of trifluoroacetophenone (**46b**), compared with acetophenone (**46a**) was observed [139] by ^{13}C NMR when a 1:1 mixture of **46a** and **46b** was treated with $BF_3 \cdot OEt_2$. Thus, a 16.7 ppm downfield shift took place only for the carbonyl carbon atom of **46a**, showing the coordination of the carbonyl group to the Lewis acid, while no change in the ^{13}C chemical shift was observed for **46b** (see Scheme 1.3). This marked difference in reactivity is attributed to the substantially decreased basicity of the carbonyl oxygen in **46b** caused by the strong inductive effect of the trifluoromethyl moiety. This selectivity was demonstrated in the highly chemoselective reduction of **46a** and **46b** under two different reaction conditions, as illustrated in Scheme 1.3. Thus, the reduction of a 1:1 mixture of **46a** and **46b** with tributyltin hydride gave 1-phenyl-2,2,2-trifluoroethanol (**48b**) as the sole product in 40% yield, while the same reaction in the presence of one equivalent of $BF_3 \cdot OEt_2$ at –78 °C afforded 1-phenylethanol (**48a**) exclusively in 82% yield.

Table 1.9 *Calculated HOMO and LUMO levels of fluorinated acetones*[a]

Compound	Energy Level (eV)		Charges		^{13}C NMR chemical shift of *C*=O
	HOMO	LUMO	*C*=O	C=*O*	
$CH_3C(O)CH_3$	–7.054	–0.784	0.573	–0.553	206.58[b]
$CH_2FC(O)CH_3$	–7.507	–1.247	0.544	–0.547	205.62[c]
$CHF_2C(O)CH_3$	–7.911	–1.873	0.518	–0.513	197.38[c]
$CF_3C(O)CH_3$	–8.278	–2.098	0.505	–0.486	189.33[c]
$CF_3C(O)CF_3$	–9.384	–3.476	0.421	–0.419	172.83[b]

[a] Computation was carried out by one of the authors (T.Y.) using the Gaussian 03W at the B3LYP/6–311++G** level.
[b] Ref. [132].
[c] Ref. [140].

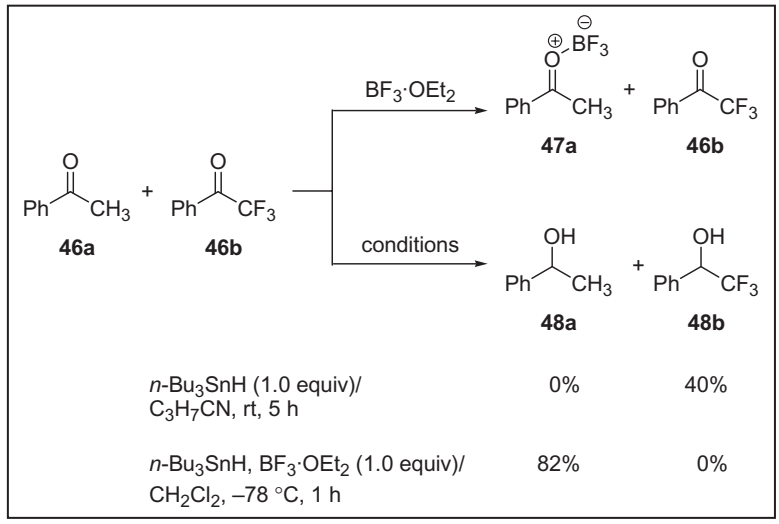

Scheme 1.3 *Reactions of* ***46a*** *and* ***46b*** *with* $BF_3 \cdot OEt_2$ *and* n-Bu_3SnH.

1.1.11 Use of Difluoromethyl and Trifluoromethyl Ketones as Transition State Analogues in Enzyme Inhibition

Tetrahedral transition state analogues of ester and amide substrates are known to function as efficient enzyme inhibitors of hydrolytic enzymes such as serine and aspartyl proteases as well as metalloproteinases (see Fig. 1.24) [141–144]. Although ketals of alkyl or aryl ketones are usually not stable, those of difluroalkyl or trifluoromethyl ketones have considerable stability, as exemplified by their facile formations of the corresponding stable hydrates [145, 146]. Therefore, substrate analogues, containing difluoroalkyl or trifluoromethyl ketone moiety in appropriate positions, have been studied as effective transition state inhibitors of hydrolytic enzymes [141, 147–150].

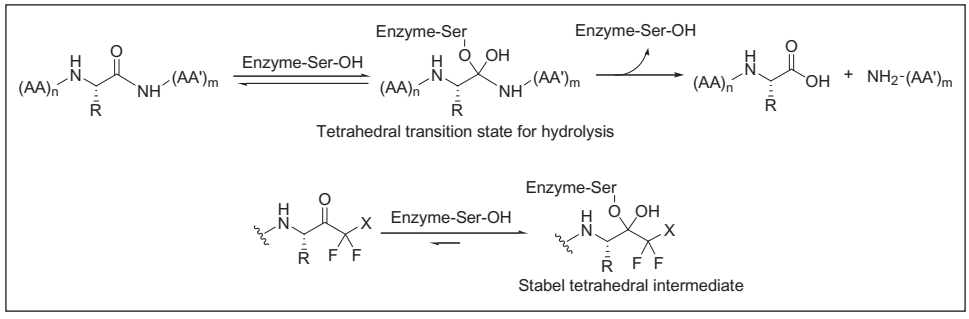

Figure 1.24 *Mechanism of peptide hydrolysis by a serine protease and enzyme inhibition by forming stable tetrahedral intermediate.*

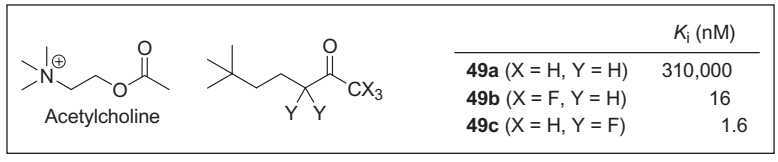

	K_i (nM)
49a (X = H, Y = H)	310,000
49b (X = F, Y = H)	16
49c (X = H, Y = F)	1.6

Figure 1.25 *Transition state inhibitors of AchE based on difluoroalkyl and trifluoromethyl ketone substrate analogues.*

For example, the rather simple difluoroalkyl ketone **49c** and trifluoromethyl ketone **49b** were designed as inhibitors of acetylcholinesterase (AchE), a serine esterase [151]. As Figure 1.25 shows, these fluoroketones exhibit excellent AchE inhibitory activities with nanomolar level K_i values, and **49c** possesses 200,000 times higher potency (K_i = 1.6 nM) than the corresponding alkyl ketone **49a** [151]. This remarkable result can be readily rationalized by taking into account the strong electrophilicity of the carbonyl group of difluoroalkyl and trifluoromethyl ketones, described in the preceding section.

In a similar manner, a variety of transition state analogues bearing a trifluoroacetyl moiety as the key functional group have been designed and synthesized as the inhibitors of human neutrophil elastase [152, 153], human cytomegalovirus protease [154, 155], human leukocyte elastase [156, 157], and other enzymes. Some of these inhibitors exhibit extremely high potency. For example, **51** has a K_i of 3.7 pM against AchE [158] and **50** has an IC_{50} of 0.88 nM against insect juvenile hormone esterase [159] (see Figure 1.26).

Difluoroalkyl ketones have also been successfully employed as the key structure of renin inhibitors. Renin is an aspartyl protease and transforms angiotensinogen (452 amino acid residues for human) to angiotensin I, which is further cleaved by angiotensin-converting enzyme (ACE) to angiotensin II, which exerts a vasoconstricting effect [160]. Accordingly, renin inhibitors have been extensively studied for their use in controlling hypertension. Although human angiotensinogen has 452 amino acid residues, the first dodecapeptide sequence is the most important for its activity (see Figure 1.27) [160].

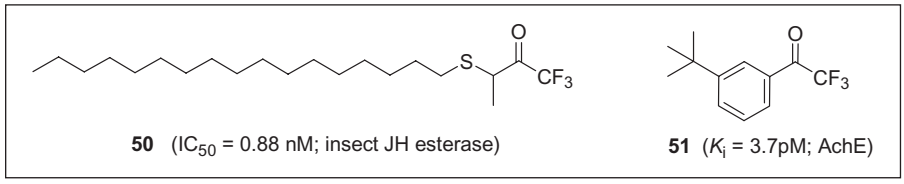

50 (IC_{50} = 0.88 nM; insect JH esterase) **51** (K_i = 3.7pM; AchE)

Figure 1.26 *Highly active transition state inhibitors bearing a trifluoroacetyl moiety.*

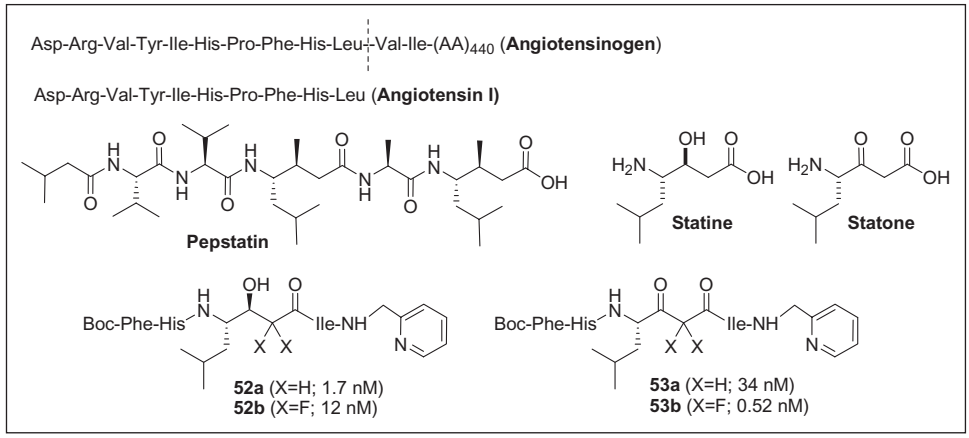

Figure 1.27 *Renin inhibitors containing difluorostatine and difluorostatone residues.*

Renin cleaves the Leu[10]-Val[11] linkage of angiotensinogen to generate angiotensin I. Thus, the tetrahedral transition state analogues of this peptide sequence should act as excellent renin inhibitors. In addition, the naturally occurring aspartyl peptidase inhibitor pepstatin [161], active against renin, contains a unique non-proteinogenic amino acid residue, "statine," which mimics the tetradedral transition state (see Figure 1.27) [162]. Accordingly, peptidomimetics, containing difluorostatine residue and its oxidized form, difluorostatone residue, have been synthesized and their activities evaluated. For example, difluorostatine-containing **52b** and difluorostatone-containing **53b** represent this class of renin inhibitors (see Figure 1.27) [163, 164]. In comparison with the corresponding hydrocarbon counterparts **52a** and **53a, 52b** shows several times reduced potency, while **53b** exhibits 65 times enhanced potency [163]. Apparently, the difluoromethylene group of **52b** reduces the basicity of the hydroxyl group, which would be counterproductive if this hydroxyl group acts as a hydrogen-bond acceptor, which explains the reduced potency of **52b** as compared to **52a**. In contrast, the difluorostatone moiety of **53b** should form a stable ketal with a water molecule, which mimics the tetrahedral transition state very well, which is the most likely reason for the two orders of magnitude enhancement in potency as compared to **53a**.

1.2 The Use of ^{19}F and ^{18}F Probes in Biophysical and Analytical Methods Relevant to Bioorganic and Medicinal Chemistry

1.2.1 ^{19}F NMR Spectroscopy

Fluorine-19 is an attractive probe nucleus for NMR because of its relatively small size, a nuclear spin of 1/2, natural abundance, high NMR sensitivity, and pronounced long-range effects. Solid-state ^{19}F NMR is an excellent tool for studying membrane-active peptides in their lipid-bound environment. The prerequisite of ^{19}F NMR experiments is the inclusion of a specific ^{19}F-reporter group into peptides and proteins. In structural studies, the most preferable labeling is with CF_3-groups that are rigidly attached to the peptide backbone. Problems of ^{19}F-labeled amino acid incorporation, including HF-elimination, racemization, and slow coupling, can easily be overcome. ^{19}F NMR data analysis will provide information about conformational changes, the structure and orientation of peptides, or the kinetics of ligand binding, properties that are intimately related to the function of the peptide. For example, solid-state ^{19}F NMR spectroscopy revealed that Trp41 participates in the gating mechanism of the M2 proton channel of influenza A virus [165] (see Figure 1.28). The integral membrane protein M2 of influenza A virus assembles as a tetrameric bundle to form a proton-conducting channel that is activated by low pH. A synthetic 25-residue peptide containing the M2 transmembrane (TM) domain was labeled with 6F-Trp41 and studied in lipid membranes by solid-state ^{19}F NMR. Through this solid-state ^{19}F NMR analysis in combination with computational energy calculations, it was demonstrated that the side-chain conformation and position of Trp41 differs significantly in the two pH-dependent states of the proton channel of the TM domain of the M2 protein, suggesting that the four tryptophan residues actively participate in activating the channel mechanically.

In another application, ^{19}F NMR studies have provided critical information on the bioactive conformation of taxoids. Fluorine-containing taxoids have been used as probes for NMR analysis of the conformational dynamics of paclitaxel in conjunction with molecular modeling [166]. The dependence of the ^{19}F chemical shifts and the $J_{H2'-H3'}$ values of these fluorinated analogues is examined through ^{19}F and ^{1}H variable-temperature (VT) NMR measurements. The experiments clearly indicate highly dynamic behavior of these molecules and the existence of equilibrium between conformers. The analysis of the VT NMR data in combination with molecular modeling, including restrained molecular dynamics (RMD), has identified three key conformers, which were further confirmed by the ^{19}F–^{1}H heteronuclear NOE measurements.

Fluorine-probe protocol has been applied to solid-state magic-angle spinning (SSMAS) ^{19}F NMR analysis with the radiofrequency-driven dipolar recoupling (RFDR) method to measure the F–F distance in the microtubule-bound conformation of F_2-10-Ac-docetaxel (see Figure 1.29a) [167]. Moreover, five intramolecular distances of the key atoms in the microtubule-bound $^{19}F/^{2}H/^{13}C$-labeled paclitaxel were determined by the rotational echo double resonance (REDOR) method (see Figure 1.29b and c) [168, 169].

1.2.2 *In vivo* ^{19}F Magnetic Resonance Spectroscopy

Magnetic resonance (MR) spectroscopy is used to measure the levels of different metabolites in body tissues. With the increasing popularity of fluorinated compounds in

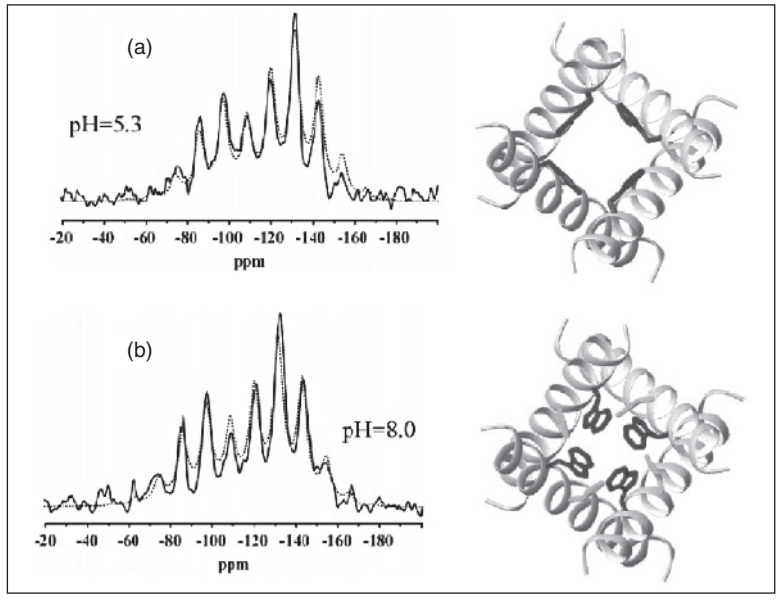

Figure 1.28 *Experimental (solid lines) and simulated (dashed lines) spin-echo spectra of 6F-Trp41-M2TMD at 6.5 kHz MAS at pH 5.3 (a) and pH 8.0 (b). Side-chain conformations (bottom view) of Trp41 (blue) and His37 (green) in the TM channel structure of the homotetrameric M2 protein are shown to the right side of the spectra. At pH 8.0, the structural parameters implicate an inactivated state, while at pH 5.3 the tryptophan conformation represents the activated state. See color plate 1.28.*
*(*Source: *Reprinted with permission from Witter, R., Nozirov, F., Sternberg, U., Cross, T. A., Ulrich, A. S., and Fu, R. Solid-state ^{19}F NMR spectroscopy reveals that Trp41 participates in the gating mechanism of the M2 proton channel of influenza A virus,* J. Am. Chem. Soc. *(2008)* **130***, 918–924. Copyright (2008) American Chemical Society.)*

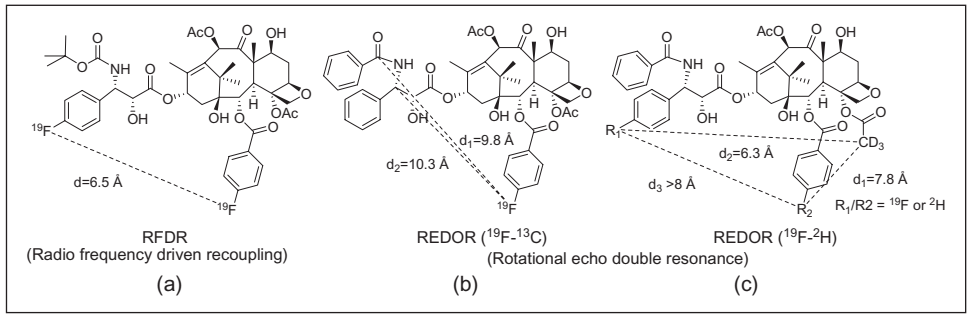

Figure 1.29 *Solid-state NMR studies on the microtubule-bound conformation of taxoids using fluoro-taxoid probes.*

pharmaceutical research, *in vivo* ^{19}F MR spectroscopy has become a valuable tool for identifying and monitoring fluorinated compounds and metabolites. Although almost all ^{19}F MR examinations are limited by the relatively low signal–noise ratio (SNR) of the spectra, ^{19}F MR spectroscopy has a unique role in clinical research applications and is complementary to other structural and functional imaging tools. It is able to identify and measure fluorine-containing drugs and their metabolites in biofluids due in part to the lack of naturally occurring MR-visible fluorine metabolites. In addition, it is noninvasive and therefore provides options for investigating the long-term disposition of pharmaceuticals. A wide range of fluorine-containing pharmaceuticals and metabolites have been evaluated in patients using *in vivo* ^{19}F MR spectroscopy. The most frequently examined organs have been the brain and the liver, although heart and extremity muscle, as well as bone marrow, have also been evaluated. Assessment of fluorine-containing drugs using human *in vivo* fluorine (^{19}F) MR spectroscopy has proved to be an important technique in drug design and preclinical studies. One good example is seen in the application of ^{19}F NMR to metabolic studies of capecitabine, the recently developed oral prodrug of 5-fluorouracil [170].

The degradation pathway of capecitabine, incorporating the new fluorinated metabolites found in urine using ^{19}F NMR, is depicted in Figure 1.30, and a typical ^{19}F NMR spectrum of urine is presented in Figure 1.31. The mean percentage of dose excreted in urine as parent drug and its fluorinated metabolites up to 48 h post dosing, measured by ^{19}F NMR, was 84.2%, close to 92.3% of the radioactivity recovered at that time. This difference of less than 10% demonstrates that ^{19}F NMR spectroscopy is a suitable technique for quantitative studies. ^{19}F NMR was also able to measure the relevant level of each fluorinated metabolite.

1.2.3 Positron Emission Tomography

Positron emission tomography (PET) is a powerful *in vivo* imaging technique that produces three-dimensional images or maps of functional processes in the body. It is used heavily in clinical research and diagnosis, as well as in drug development. Figure 1.32 shows an example of assessing dopamine D_2 receptor availability in cocaine abusers by the use of PET [171]. When compared with normal controls, cocaine abusers showed significant decreases in dopamine D_2 receptor availability that persisted 3–4 months after detoxification, as indicated by the marked reduction in the binding of [^{18}F]*N*-methylspiroperidol in PET scans.

Since PET works by detecting pairs of γ-rays emitted directly by a positron-emitting radioisotope introduced into the body on a metabolically active molecule, the use of PET is driven by the characteristics and availability of appropriately labeled radiopharmaceuticals that are specifically designed for measurement of targeted biochemical processes. Fluorine-18 has particularly appealing properties as positron-emitting radionuclide for PET imaging: (i) addition of a fluorine atom to a large molecule can often (but not always) be accomplished without significant changes to the physiochemical or biological properties of the compound; (ii) fluorine-18 has a relatively long half-life, which permits longer synthesis times, thus opening up possibilities for multistep radiolabeling procedures, as well as the option for commercial manufacture at an offsite location.

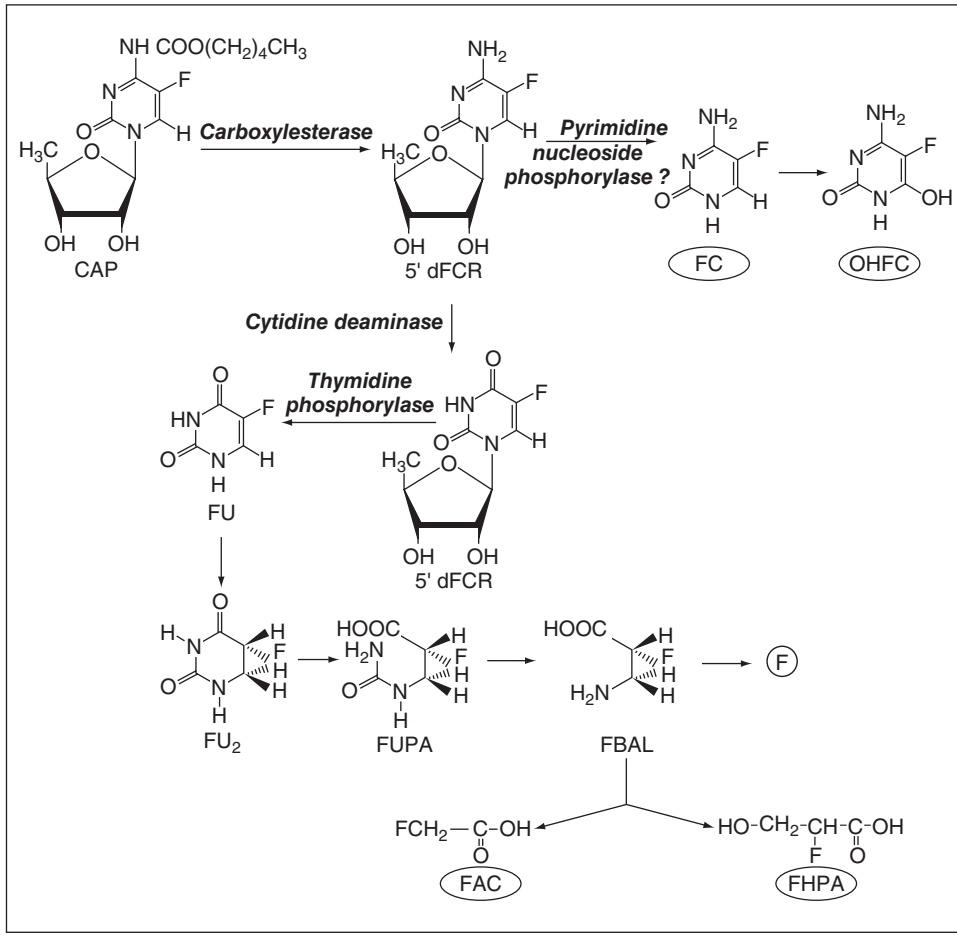

Figure 1.30 *Catabolic pathway of capecitabine from ^{19}F NMR analysis of patients' urine. All the compounds are represented in neutral form. CAP, capecitabine; 5'dFCR, 5'-deoxy-5-fluorocytidine; FC, 5-fluorocytosine; OHFC, 6-hydroxy-5-fluorocytosine; 5'dFUR, 5'-deoxy-5-fluorouridine; FU, 5-fluorouracil; FUH_2, 5,6-dihydro-5-fluorouracil; FUPA, α-fluoro-β-ureidopropionic acid; FBAL, α-fluoro-β-alanine; F^-, fluoride ion; FHPA, 2-fluoro-3-hydroxypropanoic acid; FAC, fluoroacetic acid. Metabolites identified for the first time in urine of patients with ^{19}F NMR are represented in ellipses.*

*(*Source: *Reprinted with permission from Malet-Martino, M., Gilard, V., Desmoulin, F., and Martino, R. Fluorine nuclear magnetic resonance spectroscopy of human biofluids in the field of metabolic studies of anticancer and antifungal fluoropyrimidine drugs,* Clin. Chim. Acta *(2006)* **366***, 61–73. Copyright (2006) Elsevier.)*

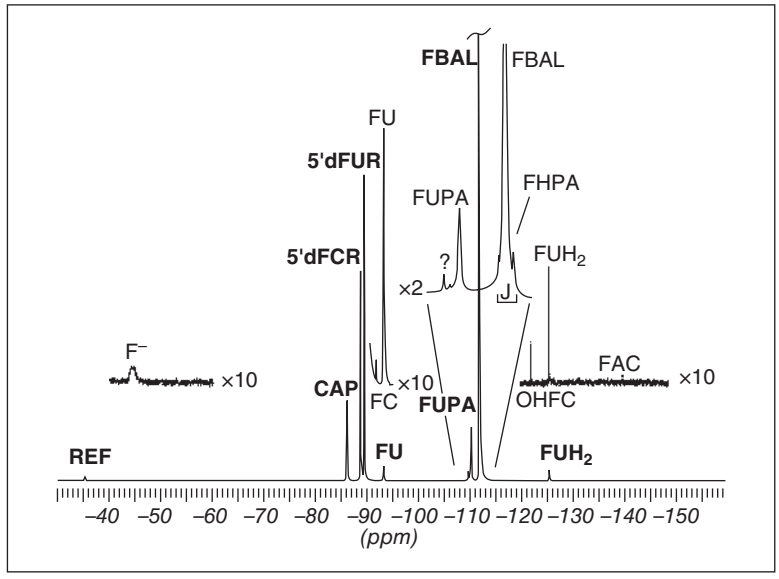

Figure 1.31 *^{19}F NMR spectrum at 282 MHz with proton decoupling of a urine sample from a patient receiving oral capecitabine at a dose of 3800 mg/day, administered twice daily at 12-hour interval, as a second treatment 3 months after the first one. Urine fraction 0–12 h collected after the first dose of 1900 mg and 10-fold concentrated, pH of the sample: 5.45. The chemical shifts are expressed relative to the resonance peak of TFA (5% w/v aqueous solution) used as external reference.*
*(*Source: *Reprinted with permission from Malet-Martino, M., Gilard, V., Desmoulin, F., and Martino, R. Fluorine nuclear magnetic resonance spectroscopy of human biofluids in the field of metabolic studies of anticancer and antifungal fluoropyrimidine drugs,* Clin Chim. Acta *(2006)* ***366****, 61–73. Copyright (2006) Elsevier.)*

Development of methods for fluorine-18 labeling has been actively pursued in the last two decades (see Figure 1.33) [172, 173]. Nucleophilic and electrophilic fluorinations have been successfully applied to generate an increasingly diverse assortment of chemical structures. Recent application of "click" chemistry and the use of protic solvents in nucleophilic fluorinations will significantly impact both the types of compounds labeled and the yields obtained.

1.3 Summary

This introductory chapter concisely summarizes the unique properties of fluorine and fluorine-containing substituents and functional groups from a physical organic chemistry point of view and then the applications of those characteristics to organic, bioorganic, and medicinal chemistry as well as chemical biology and biomedical research. The following chapters will further elaborate and discuss a wide range of topics in the rapidly expanding scope of fluorine in medicinal chemistry and chemical biology.

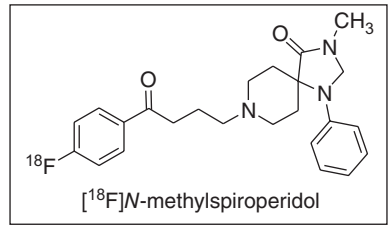

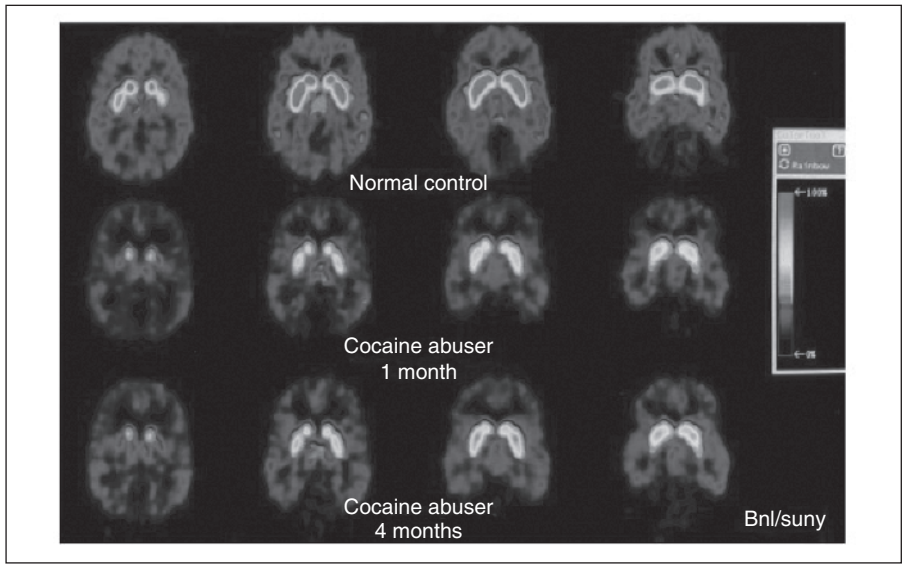

Figure 1.32 *[18F]*N*-methylspiroperidol images in a normal control and in a cocaine abuser tested 1 month and 4 months after last cocaine use. The images correspond to the four sequential planes where the basal ganglia are located. The color scale has been normalized to the injected dose. See color plate 1.32.*
*(*Source: *Volkow, N. D., Fowler, J. S., Wang, G. J., Hitzemann, R., Logan, J., Schlyer, D. J., Dewey, S. L., and Wolf, A. P. Decreased dopamine D2 receptor availability is associated with reduced frontal metabolism in cocaine abusers,* Synapse *(1993)* ***14****, 169-177. Reprinted with permission of Wiley-Liss Inc., a subsidiary of John Wiley & Sons, Inc. Copyright (1993) Wiley Interscience.)*

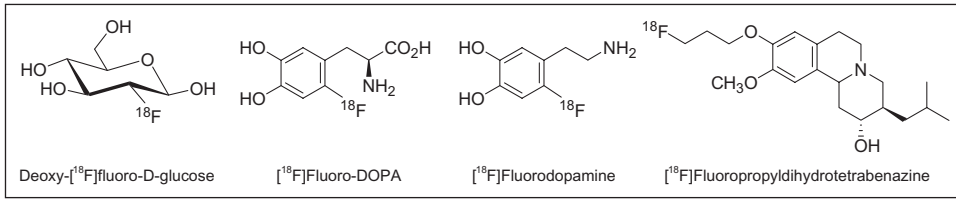

Figure 1.33 *Examples of 18F-radiopharmaceuticals.*

References

1. O'Hagan, D. and Harper, D. B. (1999) Fluorine-containing natural products. *J. Fluorine Chem.*, **100**, 127–133.
2. Fried, J. and Sabo, E. F. (1953) Synthesis of 17α-hydroxycorticosterone and its 9α-halo derivatives from 11-epi-17α-hydroxycorticosterone. *J. Am. Chem. Soc.*, **75**, 2273–2274.
3. Heidelberger, C., Chaudhuri, N. K., Danneberg, P., *et al.* (1957) Fluorinated pyrimidines, a new class of tumor-inhibitory compounds. *Nature*, **179**, 663–666.
4. *MedAdNews 200 – World's Best-Selling Medicines, MedAdNews, July 2007* (http://en.wikipedia.org/wiki/List_of_top_selling_drugs).
5. Tan, L.-S., Chen, C.-Y., Tillyer, R. D., *et al.* (1999) A novel, highly enantioselective ketone alkynylation reaction mediated by chiral zinc aminoalkoxides. *Angew. Chem. Int. Ed.*, **38**, 711–713.
6. Humphreys, J. L., Lowes, D. J., Wesson, K. A. and Whitehead, R. C. (2006) Arene *cis*-dihydrodiols – useful precursors for the preparation of antimetabolites of the shikimic acid pathway: application to the synthesis of 6,6-difluoroshikimic acid and (6*S*)-6-fluoroshikimic acid. *Tetrahedron*, **62**, 5099–5108.
7. Chou, T.-C., Dong, H.-J., Rivkin, A., *et al.* (2003) Design and total synthesis of a superior family of epothilone analogues, which eliminate xenograft tumors to a nonrelapsable state. *Angew. Chem. Int. Ed.*, **42**, 4762–4767.
8. Damon, D. B., Dugger, R. W., Magnus-Aryitey, G., *et al.* (2006) Synthesis of the CETP inhibitor torcetrapib: The resolution route and origin of stereoselectivity in the iminium ion cyclization. *Org. Process Res. Dev.*, **10**, 464–471.
9. Kim, D., Wang, L., Beconi, M., *et al.* (2005) (2*R*)-4-Oxo-4-[3-(trifluoromethyl)-5,6-dihydro [1,2,4]triazolo[4,3-a]pyrazin-7(8*H*)-yl]-1-(2,4,5-trifluorophenyl)butan-2-amine: A potent, orally active dipeptidyl peptidase IV inhibitor for the treatment of type 2 diabetes. *J. Med. Chem.*, **48**, 141–151.
10. Uneyama, K. (2006) *Organofluorine Chemistry*, Blackwell Publishing, Oxford.
11. Soloshonok, V. A., Mikami, K., Yamazaki, T., *et al.* (2006) *Current Fluoroorganic Chemistry: New Synthetic Directions, Technologies, Materials, and Biological Applications*, ACS Symposium Series 949, American Chemical Society, Washington, D. C.
12. Percy, J. M. (2006) *Science of Synthesis*, Vol. **34**. Georg Thieme Verlag, Stuttgart.
13. Soloshonok, V. A. (2005) *Fluorine-Containing Synthons*. ACS Symposium Series 911, American Chemical Society, Washington, D. C.
14. Kirsch, P. (2004) *Modern Fluoroorganic Chemistry: Synthesis, Reactivity, Applications*, Wiley-VCH Verlag, GmbH, Stuttgart.
15. Hiyama, T. (2000) *Organofluorine Compounds: Chemistry and Applications*, Springer Verlag, Stuttgart.
16. Soloshonok, V. A. (1999) *Enantiocontrolled Synthesis of Fluoroorganic Compounds – Stereochemical Challenges and Biomedicinal Targets*, John Wiley & Sons, Inc., New York.
17. Kitazume, T. and Yamazaki, T. (1998) *Experimental Methods in Organic Fluorine Chemistry*, Kodansha, Gordon and Breach Science Publisher, Tokyo.
18. Hudlicky, M. and Pavlath, A. E. (1995) *Chemistry of Organic Fluorine Compounds II – A Critical Review*, American Chemical Society, Washington, D. C.
19. Kukhar', V. P. and Soloshonok, V. A. (1995) *Fluorine-containing Amino Acids – Synthesis and Properties*, John Wiley & Sons, Inc., New York.
20. Müller, K., Faeh, C. and Diederich, F. (2007) Fluorine in Pharmaceuticals: Looking beyond intuition. *Science*, **317**, 1881–1886.

21. Isanbor, C. and O'Hagan, D. (2006) Fluorine in medicinal chemistry: A review of anti-cancer agents. *J. Fluorine Chem.*, **127**, 303–319.
22. Bégué, J.-P. and Bonnet-Delpon, D. (2006) Recent advances (1995–2005) in fluorinated pharmaceuticals based on natural products. *J. Fluorine Chem.*, **127**, 992–1012.
23. Prakesch, P., Grée, D., Chandrasekhar, S. and Grée, R. (2005) Synthesis of fluoro analogues of unsaturated fatty acids and corresponding acyclic metabolites. *Eur. J. Org. Chem.*, 1221–1232.
24. Natarajana, R., Azerada, R., Badetb, B. and Copin, E. (2005) Microbial cleavage of C–F bond. *J. Fluorine Chem.*, **126**, 425–436.
25. Böhm, H.-J., Banner, D., Bendels, S., *et al.* (2004) Fluorine in medicinal chemistry. *ChemBioChem*, **5**, 637–643.
26. Jeschke, P. (2004) The unique role of fluorine in the design of active ingredients for modern crop protection. *ChemBioChem*, **5**, 570–589.
27. Ojima, I. (2004) Use of fluorine in the medicinal chemistry and chemical biology of bioactive compounds – A case study on fluorinated taxane anticancer agents. *ChemBioChem*, **5**, 628–635.
28. Yoder, N. C. and Kumar, K. (2002) Fluorinated amino acids in protein design and engineering. *Chem. Soc. Rev.*, **31**, 335–341.
29. Smart, B. E. (2001) Fluorine substituent effects (on bioactivity). *J. Fluorine Chem.*, **109**, 3–11.
30. Dax, C., Albert, M., Ortner, J. and Paul, B. J. (2000) Synthesis of deoxyfluoro sugars from carbohydrate precursors. *Carbohydr. Res.*, **327**, 47–86.
31. Schlosser, M. (1998) Parametrization of substituents: Effects of fluorine and other heteroatoms on OH, NH, and CH acidities. *Angew. Chem. Int. Ed.*, **37**, 1496–1513.
32. O'Hagan, D. and Rzepa, H. S. (1997) Some influences of fluorine in bioorganic chemistry. *Chem. Commun.*, 645–652.
33. Bondi, A. (1964) van der Waals volumes and radii. *J. Phys. Chem.*, **68**, 441–451.
34. Lide, D. R. (2005) *Handbook of Chemistry and Physics*, 86th edn., CRC Press, New York.
35. Dean, J. A. (1999) *Lange's Handbook of Chemistry*, 15th edn., McGraw-Hill, New York.
36. (a) Peters, R. and Wakelin, R. W. (1953) Biochemistry of fluoroacetate poisoning; the isolation and some properties of the fluorotricarboxylic acid inhibitor of citrate metabolism. *Proc R. Soc. Ser. B*, **140**, 497–507. (b) Lauble, H., Kennedy, M. C., Emptage, M. H., Beinert, H., Stout, C. D., Sout, C. D. (1996) The reaction of fluorocitrate with aconitase and the crystal structure of the enzyme-inhibitor complex. *Proc. Natl. Acad. Sci. USA*, **93**, 13699–13703.
37. Black, W. C., Bayly, C. I., Davis, D. E., *et al.* (2005) Trifluoroethylamines as amide isosteres in inhibitors of cathepsin K. *Bioorg. Med. Chem. Lett.*, **15**, 4741–4744.
38. Barker, M., Clackers, M., Demaine, D. A., *et al.* (2005) Design and synthesis of new nonsteroidal glucocorticoid modulators through application of an "agreement docking" method. *J. Med. Chem.*, **48**, 4507–4510.
39. DeLuca, H. F. and Schnoes, H. K. (1984) Vitamin D: metabolism and mechanism of action. *Annu. Rep. Med. Chem.*, **19**, 179–190.
40. Kobayashi, Y. and Taguchi, T. (1985) Fluorine-modified vitamin D_3 analogs. *J. Synth. Org. Chem. Jpn.*, **43**, 1073–1082.
41. Okamoto, S., Tanaka, Y., DeLuca, H. F., *et al.* (1983) Biological activity of 24,24-difluoro-1,25-dihydroxyvitamin D_3. *Am. J. Physiol.*, **244**, E159–163.
42. Bush, I. E. and Mahesh, V. B. (1964) Metabolism of 11-oxygenated steroids. III. Some 1-dehydro and 9α-fluoro steroids. *Biochem. J.*, **93**, 236–255.
43. Wettstein, A. (1972) Chemistry of fluorosteroids and their hormonal properties, in *A Ciba Foundation Symposium: Carbon–Fluorine Compounds*, Elsevier Excerpta Medica, Amsterdam, pp. 281–301.
44. Taft, J. R. W. (1956) *Steric Effects in Organic Chemistry*, John Wiley & Sons, Inc., New York.

45. MacPhee, J. A., Panaye, A. and Dubois, J.-E. (1978) Steric effects – I: A critical examination of the Taft steric parameters–Es. Definition of a revised, broader and homogeneous scale. Extension to highly congested alkyl groups. *Tetrahedron*, **34**, 3553–3562.
46. Charton, M. (1975) Steric effects. I. Esterification and acid-catalyzed hydrolysis of esters. *J. Am. Chem. Soc.*, **97**, 1552–1556.
47. Hirsch, J. A. (1967) Table of conformational energies–1967. *Top. Stereochem.*, **1**, 199–222.
48. Carcenac, Y., Diter, P., Wakselman, C. and Tordeux, M. (2006) Experimental determination of the conformational free energies (A values) of fluorinated substituents in cyclohexane by dynamic ^{19}F NMR spectroscopy. Part 1. Description of the method for the trifluoromethyl group. *New J. Chem.*, **30**, 442–446.
49. Carcenac, Y., Tordeux, M., Wakselman, C. and Diter, P. (2006) Experimental determination of the conformational free energies (A values) of fluorinated substituents in cyclohexane by dynamic ^{19}F NMR spectroscopy. Part 2. Extension to fluoromethyl, difluoromethyl,pentafluor oethyl, trifluoromethylthio and trifluoromethoxy groups. *New J. Chem.*, **30**, 447–457.
50. Juaristi, E. (1991) *Introduction to Stereochemistry and Conformational Analysis*, John Wiley & Sons, Inc., New York.
51. Bott, G., Field, L. D. and Sternhell, S. (1980) Steric effect. A study of a rationally designed system. *J. Am. Chem. Soc.*, **102**, 5618–5626.
52. Wolf, C., König, W. A. and Roussel, C. (1995) Influence of substituents on the rotational energy barrier of atropisomeric biphenyls – Studies by polarimetry and dynamic gas chlomatography. *Liebigs Ann.*, 781–786.
53. Leroux, F. (2004) Atropisomerism, biphenyls, and fluorine: A comparison of rotational barriers and twist angles. *ChemBioChem*, **5**, 644–649.
54. Hansch, C., Leo, A. and Hoekman, D. H. (1995) *Exploring QSAR: Fundamentals and Applications in Chemistry and Biology*, American Chemical Society, Washington, D. C.
55. Hansch, C., Leo, A. and Hoekman, D. H. (1995) *Exploring QSAR: Hydrophobic, electronic, and steric constants*, American Chemical Society, Washington, D. C.
56. Hansch, C. and Leo, A. (1979) *Substituent Constants for Correlation Analysis in Chemistry and Biology*, John Wiley & Sons, Inc., Hoboken.
57. Ganguly, T., Mal, S. and Mukherjee, S. (1983) Hydrogen bonding ability of fluoroalcohols. *Spectrochim. Acta, Part A* **39A**, 657–660.
58. Morgenthaler, M., Schweizer, E., Hoffmann-Roder, A., *et al.* (2007) Predicting and tuning physicochemical properties in lead optimization: amine basicities. *ChemMedChem*, **2**, 1100–1115.
59. Abraham, M. H., Grellier, P. L., Prior, D. V., *et al.* (1989) Hydrogen bonding. Part 7. A scale of solute hydrogen-bond acidity based on log *K* values for complexation in tetrachloromethane. *J. Chem. Soc. Perkin Trans.* **2**, 699–711.
60. Van Niel, M. B., Collins, I., Beer, M. S., *et al.* (1999) Fluorination of 3-(3-(piperidin-1-yl)propyl)indoles and 3-(3-(piperazin-1-yl)propyl)indoles gives selective human 5-HT1D receptor ligands with improved pharmacokinetic profiles. *J. Med. Chem.*, **42**, 2087–2104.
61. Maren, T. and Conroy, C. W. (1993) A new class of carbonic anhydrase inhibitor. *J. Biol. Chem.*, **268**, 26233–26239.
62. Kim, C.-Y., Chang, J.-S., Doyon, J. B., *et al.* (2000) Contribution of fluorine to protein-ligand affinity in the binding of fluoroaromatic inhibitors to carbonic anhydrase II. *J. Am. Chem. Soc.*, **122**, 12125–12134.
63. Smart, B. E. (1986) Fluorinated organic molecules, in *Molecular Structure and Energetics* (eds. F. Liebman and A. Greenberg), Wiley–VCH Verlag GbmbH, Weinheim.
64. Bock, C. W., George, P., Mains, G. J. and Trachtman, M. (1979) An ab initio study of the stability of the symmetrical and unsymmetrical difluoroethylenes relative to ethylene and monofluoroethylene. *J. Chem. Soc., Perkin Trans.* **2**, 814–821.

65. Klaboe, P. and Nielsen, J. R. (1960) Infrared and Raman spectra of fluorinated ethanes. XIII. 1,2-Difluoroethane. *J. Chem. Phys.*, **33**, 1764–1774.
66. Hirano, T., Nonoyama, S., Miyajima, T., *et al.* (1986) Gas-phase fluorine-19 and proton high-resolution NMR spectroscopy: application to the study of unperturbed conformational energies of 1,2-difluoroethane. *J. Chem. Soc., Chem. Commun.*, 606–607.
67. Fernholt, L. and Kveseth, K. (1980) Conformational analysis. The temperature effect on the structure and composition of the rotational conformers of 1,2-difluoroethane as studied by gas electron diffraction. *Acta Chem. Scand. A.*, **34**, 163–170.
68. Friesen, D. and Hedberg, K. (1980) Conformational analysis. 7. 1,2-Difluoroethane. An electron-diffraction investigation of the molecular structure, composition, trans-gauche energy and entropy differences, and potential hindering internal rotation. *J. Am. Chem. Soc.*, **102**, 3987–3994.
69. Dixon, D. A., Matsuzawa, N. and Walker, S. C. (1992) Conformational analysis of 1,2-dihaloethanes: a comparison of theoretical methods. *J. Phys. Chem.*, **96**, 10740–10746.
70. Wiberg, K. B., Keith, T. A., Frisch, M. J. and Murcko, M. (1995) Solvent effects on 1,2-dihaloethane gauche/trans ratios. *J. Phys. Chem.*, **99**, 9072–9079.
71. Rablen, P. R., Hoffmann, R. W., Hrovat, D. A. and Borden, W. T. (1999) Is hyperconjugation responsible for the "gauch effect" in 1-fluoropropane and other 2-substituted-1-fluoroethanes? *J. Chem. Soc., Perkin Trans. 2*, 1719–1726.
72. Hagen, K. and Hedberg, K. (1973) Conformational analysis. III. Molecular structure and composition of 2-fluoroethanol as determined by electron diffraction. *J. Am. Chem. Soc.*, **95**, 8263–8266.
73. Huang, J.-F. and Hedberg, K. (1989) Conformational analysis. 13. 2-Fluoroethanol. An investigation of the molecular structure and conformational composition at 20, 156, and 240°. Estimate of the anti-gauche energy difference. *J. Am. Chem. Soc.*, **111**, 6909–6913.
74. Chitale, S. M. and Jose, C. I. (1986) Infrared studies and thermodynamics of hydrogen bonding in 2-halogenoethanols and 3-halogenopropanols. *J. Chem. Soc., Faraday Trans. 1*, **82**, 663–679.
75. Bakke, J. M., Bjerkeseth, L. H., Rønnow, T. E. C. L. and Steinsvoll, K. (1994) The conformation of 2-fluoroethanol – is intramolecular hydrogen bonding important? *J. Mol. Struct.*, **321**, 205–214.
76. Hoppilliard, Y. and Solgadi, D. (1980) Conformational analysis of 2-haloethanols and 2-methoxyethyl halides in a photoelectron-spectrometer. The interpretation of spectra by "ab initio" calculations. *Tetrahedron*, **36**, 377–380.
77. Michel, D., Witschard, M. and Schlosser, M. (1997) No evidence for intramolecular hydrogen bonds in α-fluorocarboxamides. *Liebigs Ann.*, 517–519.
78. Abraham, R. J. and Monasterios, J. R. (1973) Rotational isomerism. XVI. AA′BB′X NMR spectrum and rotational isomerism of 2-fluoroethyl trichloroacetate. *Org. Magn. Reson.*, **5**, 305–310.
79. Schüler, M., O'Hagan, D. and Slawin, A. M. Z. (2005) The vicinal F–C–C–F moiety as a tool for influencing peptide conformation. *Chem. Commun.*, 4324–4326.
80. Tavasli, M., O'Hagan, D., Pearson, C. and Petty, M. (2002) The fluorine gauche effect. Langmuir isotherms report the relative conformational stability of (±)-erythro- and (±)-threo-9,10-difluorostearic acids. *Chem. Commun.*, 1226–1227.
81. Briggs, C. R. S., O'Hagan, D., Howard, J. A. K. and Yufit, D. S. (2003) The C–F bond as a tool in the conformational control of amides. *J. Fluorine Chem.*, **119**, 9–13.
82. Nicoletti, M., O'Hagan, D. and Slawin, A. M. Z. (2005) α,β,γ-Trifluoroalkanes: A stereoselective synthesis placing three vicinal fluorines along a hydrocarbon chain. *J. Am. Chem. Soc.*, **127**, 482–483.
83. Hunter, L., O'Hagan, D. and Slawin, A. M. Z. (2006) Enantioselective synthesis of an all-syn vicinal fluorine motif. *J. Am. Chem. Soc.*, **128**, 16422–16423.

84. Hunter, L., Slawin, A. M. Z., Kirsch, P. and O'Hagan, D. (2007) Synthesis and conformation of multi-vicinal fluoroalkane diastereomers, *Angew. Chem. Int. Ed.*, **46**, 7887–7890.
85. DeRider, M. L., Wilkens, S. J., Waddell, M. J., *et al.* (2002) Collagen stability: Insights from NMR spectroscopic and hybrid density functional computational investigations of the effect of electronegative substituents on prolyl ring conformations. *J. Am. Chem. Soc.*, **124**, 2497–2505.
86. Apeloig, Y. (1981) Negative fluorine hyperconjugation. A theoretical re-examination. *J. Chem. Soc., Chem. Commun.*, 396–398.
87. Rahman, M. M. and Lemal, D. M. (1988) Negative hyperconjugation. The rotation-Inversion barrier in α-fluoroamines. *J. Am. Chem. Soc.*, **110**, 1964–1966.
88. Schneider, W. F., Nance, B. I. and Wallington, T. J. (1995) Bond strength trends in halogenated methanols: Evidence for negative hyperconjugation? *J. Am. Chem. Soc.*, **117**, 478–485.
89. Raabe, G., Gais, H.-J. and Fleischhauer, J. (1996) Ab initio study of fluorination upon the structure and configurational stability of α-sulfonyl carbanions: The role of negative hyperconjugation. *J. Am. Chem. Soc.*, **118**, 4622–4630.
90. Farnham, W. B., Smart, B. E., Middleton, W. J., *et al.* (1985) Crystal and molecular structure of $[(CH_3)_2N]_3S^+CF_3O^-$. Evidence for negative fluorine hyperconjugation. *J. Am. Chem. Soc.*, **107**, 4565–4567.
91. Barbarich, T. J., Rithner, C. D., Miller, S. M., *et al.* (1999) Significant inter- and intramolecular O–H···FC hydrogen bonding. *J. Am. Chem. Soc.*, **121**, 4280–4281.
92. Katagiri, T. and Uneyama, K. (2001) Chiral recognition by multicenter single proton hydrogen bonding of trifluorolactates. *Chem. Lett.*, 1330–1331.
93. Bartolomé, C., Espinet, P. and Martín-Alvarez, J. M. (2007) Is there any bona fide example of O–H···F–C bond in solution? The cases of $HOC(CF_3)_2(4\text{-}X\text{-}2,6\text{-}C_6H_2(CF_3)_2)$ (X = $Si(i\text{-}Pr)_3$, CF_3). *Chem. Commun.*, 4384–4386.
94. Pham, M., Gdaniec, M. and Polonski, T. (1998) Three-center CF···HN intramolecular hydrogen bonding in the 2,6-bis(2,6-difluorophenyl)piperidine systems. *J. Org. Chem.*, **63**, 3731–3734.
95. Li, C., Ren, S.-F., Hou, J.-L., *et al.* (2005) F···H–N Hydrogen bonding driven foldamers: Efficient receptors for dialkylammonium ions. *Angew. Chem. Int. Ed. Engl.*, **44**, 5725–5729.
96. Banks, J. W., Batsanov, A. S., Howard, J. A. K., *et al.* (1999) The preferred conformation of α-fluoroamides. *J. Chem. Soc., Perkin Trans. 2*, 2409–2411.
97. Thalladi, V. R., Weiss, H.-C., Bläser, D., *et al.* (1998) C–H···F Interactions in the crystal structures of some fluorobenzenes. *J. Am. Chem. Soc.*, **120**, 8702–8710.
98. Sosnovskikh, V. Y., Irgashev, R. A., Khalymbadzha, I. A. and Slepukhin, P. A. (2007) Stereoselective hetero-Diels–Alder reaction of 3-(trifluoroacetyl)chromones with cyclic enol ethers: synthesis of 3-aroyl-2-(trifluoromethyl)pyridines with ω-hydroxyalkyl groups. *Tetrahedron Lett.*, **48**, 6297–6300.
99. Wagner, T., Afshar, C. E., Carrell, H. L., *et al.* (1999) Difluoromethylcobalamin: Structural aspects of an old tree with a new branch. *Inorg. Chem.*, **38**, 1785–1794.
100. Erickson, J. A. and McLoughlin, J. I. (1995) Hydrogen bond donor properties of the difluoromethyl group. *J. Org. Chem.*, **60**, 1626–1631.
101. Paulini, R., Müller, K. and Diederich, F. (2005) Orthogonal multipolar interactions in structure chemistry and biology. *Angew. Chem. Int. Ed.*, **44**, 1788–1805.
102. Wang, Z., Canagarajah, B. J., Boehm, J. C., *et al.* (1998) Structural basis of inhibitor selectivity in MAP kinases. *Structure*, **6**, 1117–1128.
103. Schweizer, E., Hoffmann-Roder, A., Scharer, K., *et al.* (2006) A fluorine scan at the catalytic center of thrombin: C–F, C–OH, and C–OMe bioisosterism and fluorine effects on pK_a and log *D* values. *Chem. Med. Chem.*, **1**, 611–621.

104. Schweizer, E., Hoffmann-Roeder, A., Olsen, J. A., *et al.* (2006) Multipolar interactions in the D pocket of thrombin: large differences between tricyclic imide and lactam inhibitors. *Org. Biomol. Chem.*, **4**, 2364–2375.
105. Olsen, J. A., Banner, D. W., Seiler, P., *et al.* (2004) Fluorine interactions at the thrombin active site: Protein backbone fragments H–Cα–C=O comprise a favorable C–F environment and interactions of C–F with electrophiles. *ChemBioChem*, **5**, 666–675.
106. Olsen, J. A., Banner, D. W., Seiler, P., *et al.* (2003) A fluorine scan of thrombin inhibitors to map the fluorophilicity/fluorophobicity of an enzyme active site: Evidence for C–F···C=O interactions. *Angew. Chem. Int. Ed.*, **42**, 2507–2511.
107. Berman, H. M., Westbrook, J., Feng, Z., *et al.* (2000) The protein data bank. *Nucleic Acids Res.*, **28**, 235–242.
108. Hughes, D. L., Sieker, L. C., Bieth, J. and Dimicoli, J. L. (1982) Crystallographic study of the binding of a trifluoroacetyl dipeptide anilide inhibitor with elastase. *J. Mol. Biol.*, **162**, 645–658.
109. Adler, M., Davey, D. D., Phillips, G. B., *et al.* (2000) Preparation, characterization, and the crystal structure of the inhibitor ZK-807834 (CI-1031) complexed with factor Xa. *Biochemistry*, **39**, 12534–12542.
110. Mattos, C., Giammona, D. A., Petsko, G. A. and Ringe, D. (1995) Structural analysis of the active site of porcine pancreatic elastase based on the X-ray crystal structures of complexes with trifluoroacetyl-dipeptide-anilide inhibitors. *Biochemistry*, **34**, 3193–3203.
111. Fischer, F. R., Schweizer, W. B. and Diederich, F. (2007) Molecular torsion balance: Evidence for favorable orthogonal dipolar interactions between organic fluorine and amide groups. *Angew. Chem. Int. Ed.*, **46**, 8270–8273.
112. Roth, B. D., Ortwine, D. F., Hoefle, M. L., *et al.* (1990) Inhibitors of cholesterol biosynthesis., 1. trans-6-(2-Pyrrol-1-ylethyl)-4-hydroxypyran-2-ones, a novel series of HMG-CoA reductase inhibitors. 1. Effects of structural modifications at the 2- and 5-positions of the pyrrole nucleus. *J. Med. Chem.*, **33**, 21–31.
113. Istvan, E. S. and Deisenhofer, J. (2001) Structural mechanism for statin inhibition of HMG-CoA reductase. *Science*, **292**, 1160–1164.
114. Langmuir, I. (1919) Isomorphism, isosterism and covalence. *J. Am. Chem. Soc.*, **41**, 1543–1559.
115. Hann, M. M., Sammes, P. G., Kennewell, P. D. and Taylor, J. B. (1980) On double bond isosteres of the peptide bond: an enkephalin analog. *J. Chem. Soc., Chem. Commun.*, 234–235.
116. Allmendinger, T., Furet, P. and Hungerbuhler, E. (1990) Fluoroolefin dipeptide isosteres. – I. The synthesis of GlyΨ(CF = CH)Gly and racemic PheΨ(CF = CH)Gly. *Tetrahedron Lett.*, **31**, 7297–7300.
117. Frisch, M. J., Trucks, G. W., Schlegel, H. B., *et al.* (2004) Gaussian 03 Release Notes, http://www.gaussian.com/g_tech/g03_rel.htm, Gaussian, Inc., Wallingford CT.
118. Datar, P., Srivastava, S., Coutinho, E. and Govil, G. (2004) Substance P: structure, function, and therapeutics. *Curr. Top. Med. Chem.*, **4**, 75–103.
119. Allmendinger, T., Felder, E. and Hungerbuhler, E. (1990) Fluoroolefin dipeptide isosteres. – II. Enantioselective synthesis of both antipodes of the Phe-Gly dipeptide mimic. *Tetrahedron Lett.*, **31**, 7301–7304.
120. Xiao, J.-B., Weisblum, B. and Wipf, P. (2005) Electrostatic versus steric effects in peptidomimicry: Synthesis and secondary structure analysis of gramicidin S analogues with (*E*)-alkene peptide isosteres. *J. Am. Chem. Soc.*, **127**, 5742–5743.
121. Wipf, P., Henninger, T. C. and Geib, S. J. (1998) Methyl- and (trifluoromethyl)alkene peptide isosteres: synthesis and evaluation of their potential as β-turn promoters and peptide mimetics. *J. Org. Chem.*, **63**, 6088–6089.

122. Volonterio, A., Bravo, P. and Zanda, M. (2000) Synthesis of Partially Modified Retro and Retroinverso [NHCH(CF3)]-Peptides. *Org. Lett.*, **2**, 1827–1830.
123. Volonterio, A., Bellosta, S., Bravin, F., *et al.* (2003) Synthesis, structure and conformation of partially-modified retro- and retro-inverso [NHCH(CF_3)]Gly peptides. *Chem. Eur. J.*, **9**, 4510–4522.
124. Black, W. C., Baylya, C. I., Davisc, D. E., *et al.* (2005) Trifluoroethylamines as amide isosteres in inhibitors of cathepsin K Bioorg. *Med. Chem. Lett.*, **15**, 4741–4744.
125. Sani, M., Volonterio, A. and Zanda, M. (2007) The trifluoroethylamine function as peptide bond replacement. *ChemMedChem*, **2**, 1693–1700.
126. Moran, S., Ren, R. X.-F., Rumney IV, S. and Kool, E. T. (1997) Difluorotoluene, a nonpolar isostere for thymine, codes specifically and efficiently for adenine in DNA replication. *J. Am. Chem. Soc.*, **119**, 2056–2057.
127. Guckian, K. M. and Kool, E. T. (1997) Highly precise shape mimicry by a difluorotoluene deoxynucleoside, a replication-component substitute for thymidine. *Angew. Chem. Int. Ed. Engl.*, **36**, 2825–2828.
128. Kool, E. T. and Sintim, H. O. (2006) The difluorotoluene debate – a decade later. *Chem. Commun.*, 3665–3675.
129. Evans, T. A. and Seddon, K. R. (1997) Hydrogen bonding in DNA – a return to the status quo. *Chem. Commun.*, 2023–2024.
130. Wang, X. and Houk, K. N. (1998) Difluorotoluene, a thymine isostere, does not hydrogen bond after all. *Chem. Commun.*, 2631–2632.
131. Blackburn, G. M., Kent, D. E. and Kolkmann, F. (1984) The synthesis and metal binding characteristics of novel, isopolar phosphonate analogs of nucleotides. *J. Chem. Soc., Perkin Trans. 1*, 1119–1125.
132. Burke, J., T. R., Kole, H. K. and Roller, P. P. (1994) Potent inhibition of insulin receptor dephosphorylation by a hexamer peptide containing the phosphotyrosyl mimetic F2pmp. *Biochem. Biophys. Res. Commun.*, **204**, 129–134.
133. Nieschalk, J. and O'Hagan, D. (1995) Monofluorophosphonates as phosphate mimics in bio-organic chemistry: a comparative study of CH_2-, CHF-, and CF_2-phosphonate analogues of sn-glycerol-3-phosphate as substrates for sn-glycerol-3-phosphate dehydrogenase. *J. Chem. Soc., Chem. Commun.*, 719–720.
134. Hakogi, T., Yamamoto, T., Fujii, S., *et al.* (2006) Synthesis of sphingomyelin difluoromethylene analogue. *Tetrahedron Lett.*, **47**, 2627–2630.
135. Hamilton, C. J., Roberts, S. M. and Shipitsin, A. (1998) Synthesis of a potent inhibitor of HIV reverse transcriptase. *Chem. Commun.*, 1087–1088.
136. Cox, R. J., Hadfield, A. T. and Mayo-Martín, M. B. (2001) Difluoromethylene analogues of aspartyl phosphate: the first synthetic inhibitors of aspartate semi-aldehyde dehydrogenase. *Chem. Commun.*, 1710–1711.
137. Xu, Y., Aoki, J., Shimizu, K., *et al.* (2005) Structure–activity relationships of fluorinated lysophosphatidic acid analogues. *J. Med. Chem.*, **48**, 3319–3327.
138. Dubowchik, G. M., Vrudhula, V. M., Dasgupta, B., *et al.* (2001) 2-Aryl-2,2-difluoroacetamide FKBP12 ligands: Synthesis and X-ray structural studies. *Org. Lett.*, **3**, 3987–3990.
139. Asao, N., Asano, T. and Yamamoto, Y. (2001) Do more electrophilic aldehydes/ketones exhibit higher reactivity toward nucleophiles in the presence of Lewis acids? *Angew. Chem. Int. Ed.*, **40**, 3206–3208.
140. Abraham, R. J., Jones, A. D., Warne, M. A., *et al.* (1996) Conformational analysis. Part 27. NMR, solvation and theoretical investigation of conformational isomerism in fluoro- and 1,1-difluoroacetone. *J. Chem. Soc., Perkin Trans. 2*, 533–539.
141. Maryanoff, B. E. and Costanzo, M. J. (2008) Inhibitors of proteases and amide hydrolases that employ an α-ketoheterocycle as a key enabling functionality. *Bioorg. Med. Chem.*, **16**, 1562–1595.

142. Westerik, J. O. and Wolfenden, R. (1971) Aldehydes as inhibitors of papain. *J. Biol. Chem.*, **247**, 8195–8197.
143. Thompson, R. C. (1973) Use of peptide aldehydes to generate transition-state analogs of elastase. *Biochemistry*, **12**, 47–51.
144. Shah, D. O., Lai, K. and Gorenstein, D. G. (1984) Carbon-13 NMR spectroscopy of "transition-state analog" complexes of *N*-acetyl-l-phenylalaninal and α-chymotrypsin. *J. Am. Chem. Soc.*, **106**, 4272–4273.
145. Hauptschein, M. and Braun, R. A. (1955) The reaction of ethyl perfluorobutyrate with sodium. An improved synthesis of perfluoroheptan-4-one. *J. Am. Chem. Soc.*, **77**, 4930–4931.
146. Husted, D. R. and Ahlbrecht, A. H. (1952) The chemistry of the perfluoro acids and their derivatives. III. The perfluoro aldehydes. *J. Am. Chem. Soc.*, **74**, 5422–5426.
147. Takahashi, L. H., Radhakrishnan, R., Rosenfield Jr., R. E., *et al.* (1989) Crystal-structure of the covalent complex formed by a peptidyl α,α-difluoro-β-ketop amide with porcine pancreatic elastase at 1.78-Å resolution. *J. Am. Chem. Soc.*, **111**, 3368–3374.
148. Brady, K., Wei, A.-Z., Ringe, D. and Abeles, R. H. (1990) Structure of chymotrypsin-trifluoromethyl ketone inhibitor complexes: Comparison of slowly and rapidly equilibrating inhibitors. *Biochemistry*, **29**, 7600–7607.
149. Takahashi, L. H., R., R., Rosenfield Jr., R. E., Meyer, Jr. E. F., *et al.* (1988) X-ray diffraction analysis of the inhibition of porcine pancreatic elastase by a peptidyl trifluoromethylketone. *J. Mol. Biol.*, **201**, 423–428.
150. Veale, C. A., Bernstein, P. R., Bryant, C., *et al.* (1995) Nonpeptidic inhibitors of human leukocyte elastase. 5. Design, synthesis, and X-ray crystallography of a series of orally active 5-aminopyrimidin-6-one-containing trifluoromethyl ketones. *J. Med. Chem.*, **38**, 98–108.
151. Gelb, M. H., Svaren, J. P. and Abeles, R. H. (1985) Fluoro ketone inhibitors of hydrolytic enzymes. *Biochemistry*, **24**, 1813–1817.
152. Peet, N. P., Burkhart, J. P., Angelastro, M. R., *et al.* (1990) Synthesis of peptidyl fluoromethyl ketones and peptidyl α-keto esters as inhibitors of porcine pancreatic elastase, human neurophil elastase, and rat and human neurophil cathepsin. *J. Med. Chem.*, **33**, 394–407.
153. Angelastro, M. R., Baugh, L. E., Bey, P., *et al.* (1994) Inhibition of human neutrophil elastase with peptidyl electrophilic ketones. 2. Orally active PG-Val-Pro-Val pentafluoroethyl ketones. *J. Med. Chem.*, **37**, 4538–4553.
154. Ogilvie, W., Bailey, M., Poupart, M.-A., *et al.* (1997) Peptidomimetic inhibitors of the human cytomegalovirus protease. *J. Med. Chem.*, **40**, 4113–4135.
155. LaPlante, S. R., Bonneau, P. R., Aubry, N., *et al.* (1999) Characterization of the human cytomegalovirus protease as an induced-fit serine protease and the implications to the design of mechanism-based inhibitors. *J. Am. Chem. Soc.*, **121**, 2974–2986.
156. Warner, P., Green, R. C., Gomes, B. and Strimpler, A. M. (1994) Non-peptidic inhibitors of human leukocyte elastase. 1. The design and synthesis of pyridone-containing inhibitors. *J. Med. Chem.*, **37**, 3090–3099.
157. Veale, C. A., Bernstein, P. R., Bohnert, C. M., *et al.* (1997) Orally active trifluoromethyl ketone inhibitors of human leukocyte elastase. *J. Med. Chem.*, **40**, 3173–3181.
158. Nair, H. K. and Quinn, D. M. (1993) m-Alkyl α,α,α-trifluoroacetophenones: A new class of potent transition state analog inhibitors of acetylcholinesterase. *Bioorg. Med. Chem. Lett.*, **3**, 2619–2622.
159. Linderman, R. J., Graves, D. M., Garg, S., *et al.* (1993) Unique inhibition of a serine esterase. *Tetrahedron Lett.*, **34**, 3227–3230.
160. Basso, N. and Terragno, N. A. (2001) History about the discovery of the renin-angiotensin system. *Hypertension*, **38**, 1246–1249.
161. Umezawa, H., Aoyagi, T., Morishima, H., *et al.* (1970) Pepstatin, a new pepsin inhibitor produced by Actinomycetes. *J. Antibiot.*, **23**, 259–262.

162. Marciniszyn, J., Hartsuck, J. A. and Tang, J. (1976) Mode of inhibition of acid proteases by pepstatin. *J. Biol. Chem.*, **251**, 7088–7094.
163. Thaisrivongs, S., Pals, D. T., Kati, W. M., *et al.* (1986) Design and synthesis of potent and specific renin inhibitors containing difluorostatine, difluorostatone, and related analogues. *J. Med. Chem.*, **29**, 2080–2087.
164. Fearon, K., Spaltenstein, A., Hopkins, P. B. and Gelb, M. H. (1987) Fluoro ketone containing peptides as inhibitors of human renin. *J. Med. Chem.*, **30**, 1617–1622.
165. Witter, R., Nozirov, F., Sternberg, U., *et al.* (2008) Solid-state ^{19}F NMR spectroscopy reveals that Trp_{41} participates in the gating mechanism of the M2 proton channel of influenza A virus. *J. Am. Chem. Soc.*, **130**, 918–924.
166. Ojima, I., Kuduk, S. D., Chakravarty, S., *et al.* (1997) A novel approach to the study of solution structures and dynamic behavior of paclitaxel and docetaxel using fluorine-containing analogs as probes. *J. Am. Chem. Soc.*, **119**, 5519–5527.
167. Ojima, I., Kuduk, S. D. and Chakravarty, S. (1998) Recent advances in the medicinal chemistry of taxoid anticancer agents. *Adv. Med. Chem.*, **4**, 69–124.
168. Li, Y., Poliks, B., Cegelski, L., *et al.* (2000) Conformation of Microtubule-Bound Paclitaxel Determined by Fluorescence Spectroscopy and REDOR NMR. *Biochemistry*, **39**, 281–291.
169. Paik, Y., Yang, C., Metaferia, B., *et al.* (2007) Rotational-echo double-resonance NMR distance measurements for the tubulin-bound paclitaxel conformation, *J. Am. Chem. Soc.*, **129**, 361–370.
170. Malet-Martino, M., Gilard, V., Desmoulin, F. and Martino, R. (2006) Fluorine nuclear magnetic resonance spectroscopy of human biofluids in the field of metabolic studies of anticancer and antifungal fluoropyrimidine drugs. *Clin. Chim. Acta*, **366**, 61–73.
171. Volkow, N. D., Fowler, J. S., Wang, G. J., *et al.* (1993) Decreased dopamine D2 receptor availability is associated with reduced frontal metabolism in cocaine abusers. *Synapse*, **14**, 169–177.
172. Ding, Y.-S. and Fowler, J. S. (1996) Fluorine-18 labeled tracers for PET studies in the neurosciences, in *Biomedical Frontiers of Fluorine Chemistry*, ACS Symposium Series 639, American Chemical Society, Washington, D. C., pp 328–343.
173. Snyder, S. E. and Kilbourn, M. R. (2003) Chemistry of fluorine-18 radiopharmaceuticals, in *Handbook of Radiopharmaceuticals* (eds. M. J. Welch and C. S. Redvanly), pp. 195–227, John Wiley & Sons, Ltd, Chichester.